University of Applied Sciences

HOCHSCHULE
EMDEN·LEER

Fachbereich Seefahrt und Maritime Wissenschaften

Jürgen Göken, Sarah Fayed

Experimental Results on the Use of Ultrasonic and Acoustic Measurements for Vibration Analysis

Schriftenreihe der Hochschule Emden/Leer, Band 29

Jürgen Göken, Sarah Fayed

Experimental Results on the Use of Ultrasonic and Acoustic Measurements for Vibration Analysis

Hochschule Emden/Leer
Emden 2019

Schriftenreihe der Hochschule Emden/Leer, Band 29

Verlag: Hochschule Emden/Leer
Druckerei: VON DER SEE, Emden
Buchbinderei: VON DER SEE, Emden

Hochschule Emden/Leer
Constantiaplatz 4
26723 Emden
E-Mail: bibliothek.emden@hs-emden-leer.de

ISBN: 978-3-944262-20-8

Experimental Results on the Use of Ultrasonic and Acoustic Measurements for Vibration Analysis

by

Prof. Dr. Jürgen Göken

&

Sarah Fayed (M.Sc.)

Laboratory of Materials Physics,

Faculty of Maritime Sciences,

University of Applied Sciences Emden/Leer, Germany

Contents

A Feasibility Study of Two Different Ultrasonic Distance Sensors for Measuring the Mechanical Deflection on Vibrating Surfaces

Prof. Dr. rer. nat. habil. Jürgen Göken, M.Sc. Sarah Fayed

University of Applied Sciences Emden-Leer, Faculty of Maritime Sciences, Bergmannstraße 36, 26789 Leer, Germany

E-mail: juergen.goeken@hs-emden-leer.de; sarah.fayed@hs-emden-leer.de

The comfort for passengers in transport vehicles such as cars, trains, planes and ships is significantly dependent on the human's hearing perception. The structure-borne noise should therefore remain below a noise level, where noises are perceived as unpleasant. This threshold depends on the pitch and thus on the frequency of the vibration. The vibration frequencies on ships occur due to several factors. Major factors include the speed of the ship, the structure of the hull and the material of which it is made, as well as the voyage conditions (for example weather, tides and swell). Most important, however, is the drive (engine speed), which sets the fundamental frequency. According to Germanischer Lloyd (GL) [1], the frequency range in which significant structural vibrations occur on board ships is between 1 and 80 Hz. Referring to Asmussen et al [2], avoiding noise is a challenge on passenger ships. Therefore, classification societies focus their own vibration studies primarily on passenger ships. In the presence of an excitation source, e.g. the ship's engine, the energy is transferred to the ship structure, so that other components start to oscillate. This in turn leads to the emission of vibrational energy to the air molecules (acoustic emission), which is perceived in some cases as disturbing noise. It has to be emphasised that acoustic measurements with commercially available microphones are not suitable for large, slow-running main engines, which produce low vibration frequencies on board. Therefore, an innovative acoustic device is necessary.

Previous measurements

Own acoustic measurements on board different passenger ships (for example [3]) aimed to localise undesired noise emission with the help of a sound source localisation systems (acoustic camera system with spiral microphone array or a highly sensitive acoustic probe) including a USB camera. The incident sound on the microphones was recorded synchronously, whereas the position and strength of the sound sources are determined indirectly (airborne noise) and shown colour-coded. The main intention of the output data analysis was the detection of sound sources at constant frequencies, which provide information about the ship's acoustics.

In order to get information about the radiation characteristics of flat surfaces, laboratory tests were carried out on an acrylic plate to clarify the complexity of the plate vibration [4]. The plate was first sprinkled with fine sand to roughly determine the vibrational pattern (detection of Chladni figures). The sand remained in areas where a node was created and displaced accordingly at the places where strong vibration amplitudes occurred. A highly sensitive sound sensor was used to measure the sound velocity at 81 equidistant points above the oscillatory plate. The plate was first firmly clamped at 16, then released at only 4 points. In further experiments, the excitation position had been changed then the plate was re-clamped. Each of the experiments showed significant changes in the oscillation patterns, which states that the oscillation pattern distinctively dependent on the excitation position and the clamping conditions. For this reason, very precise acoustic based measurements are necessary. If it is possible to determine a high-resolution vibration pattern, then it is also possible to perform selective, local structural improvements to avoid critical vibration amplitudes, and thus improve the acoustic comfort.

This work

The planned work is based on the visualization of the vibration behavior of a differently clamped plate. This makes it possible to obtain the actual oscillation pattern (distribution of antinodes and nodes) for a given external force. Since the acoustic results are already available (see [4]), an alternative measurement method based on common ultrasonic sensors should be investigated.

Ultrasonic sensors generate different elastic waves in a frequency range from 20 kHz to the megahertz range. Piezoelectric materials such as quartz, piezoceramics and selected polymers are used for this purpose. Influencing the propagation of these elastic waves through the adjacent medium, its state parameter or material properties as well as the detection of transit times or damping on the tested object determine the effects of the actual sensor. Ultrasonic sensors are suitable for the contactless detection of structure-borne noise. They are already used in large numbers in the production of modern motor vehicles with parking assistance systems. However, the resolution required for the detection of obstacles is well below the requirements for the measurement of structure-borne noise, expecting the observation of vibration patterns. The aim of this laboratory project presented here is to study the potential of two low-cost ultrasonic sensors of a documented resolution of maximum 30 mm to be used in measuring the displacement amplitudes of vibrating surfaces. For this purpose, the sensors were tested and compared with respect to their analogue and digital stability, resolution and maximum measurable frequency by means of a self-constructed experimental setup. If it becomes possible to re-

ceive a much higher resolution with the help of an appropriate signal processing or improved electronic setup, the visualisation of the vibration behaviour of differently clamped square plates should be technically feasible. This allows for the obtainment of the actual oscillation pattern (distribution of nodes and antinodes) at a given external force. The used measuring method should support the already available acoustic results that were mentioned in the last section. The obtained results could then be used as a basis for the development of an experimental set-up, which should allow the measurement of structure-borne noise by a network of up to 64 sensors for larger surfaces.

1 Experimental details and results

In this work, the two ultrasonic sensors (type HCSR04 and its successor type HYSRF05) were used. These are technically modified copies of the "Ping" sensor from Parallax [5], which is very frequently mentioned in the literature. Both sensors are commonly used because of their small size and low price. In the meantime, the sensors have been technically revised several times, so that different variants of the same type are available on the market. Due to this circumstance, the manufacturer documentation is sometimes misleading. The applied measurements were carried out with the sensor variants shown in Fig. 1. Both sensors are equipped with a Chinese 8-bit microprocessor EM78P153S [6], which works according to the so-called polling method [7]. For more information about the used sensors, please see [8].

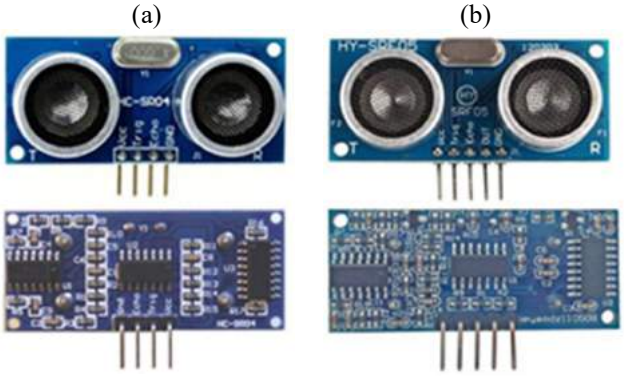

Fig. 1 Front (top) and back (bottom) sides of the used HCSR04 (a) and HYSRF05 (b) sensors [8].

The HCSR04 and the HYSRF05 transmit measurement pulses by activating only the trigger pin. If a voltage of 5 volts is applied to the microcontroller for 10 μs, the microprocessor installed on the sensor detects this and activates a charge pump. After about 260 μs, the necessary energy is available to activate the piezo elements and eight signals are transmitted at a frequency of 40 kHz [6], see Fig. 2. With the last edge (see red mark, Fig. 3) of the transmitted signal, the transit time measurement begins and results in a voltage of 5 volts being applied to the echo pin until the reflected signal is received. Over the duration of the voltage increase, the microcontroller then determines the duration of the signal.
An Arduino UNO board of the third generation (Revision 3) [9] was used to control and read out the sensors, which is equipped with a microcontroller from Atmel (type ATmega328). The suitability of these components is based on their proven high reliability and extensive documentation. The Arduino UNO has an USB and an ISCP interface in addition to the power connector. All Arduinos of the third generation have a separate microcontroller, which is responsible for communication with the computer. The microcontroller has a flash memory of 32 kilobytes and supports beside the I2C- also the SPI-communication. Overall, the controller has 20 digital ports (I / O) ports that can be used both as input and output, and six pins of the 20 ports are PWM-capable, six others can be used as an analog input [10]. In order to facilitate the communication with the development board, there is an own software development environment (IDE) with which C-programs can be written, compiled and uploaded. However, the IDE does not allow automatic backup of the data. For reading and storage, a program was therefore created in the Python programming language [11], which saves the determined data as a text file. The programs developed for microcontrollers are called sketch. These are composed of two different components, the so-called setup and loop parts. Since the sensors require a certain amount of pause between the measurements, the delay command can be used to set a defined pause time between runs of the loop part. This is important for setting the measuring frequency of the sensors.

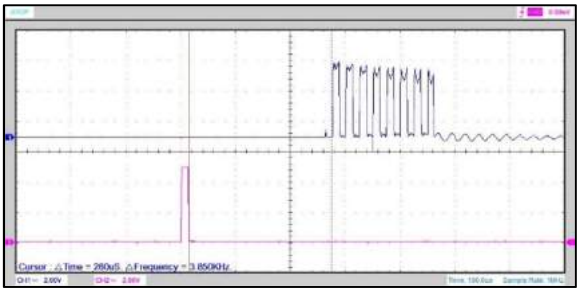

Fig. 2 Triggering signal of an ultrasonic sensor.

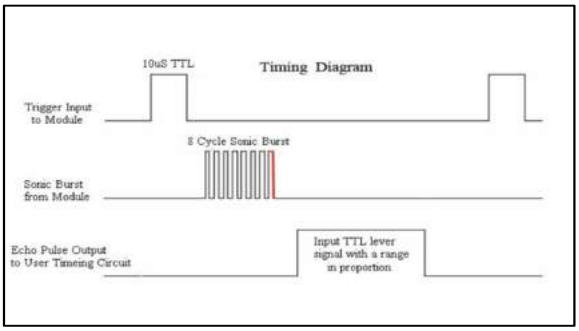

Fig. 3 Time diagram of the ultrasonic sensors.

The duration of the sound transmission (measuring time: time-of-flight of the reflected ultrasonic waves), i.e. the time difference between transmission and reception of a sound signal, is strongly dependent on the speed of sound which is on the other hand directly dependent on the temperature of the medium in which the measurement takes place (here: air). To measure the temperature of the air, the Arduino UNO was connected to a so-called NTC thermistor which works with an electrical resistance whose conductivity improves with higher temperatures. By connecting the thermistor to the microcontroller, the temperature can be measured via the voltage curve. The measuring time t as a function of the measured total distance S and temperature T (in °C) was calculated according to the equation (3) [12]. Since t corresponds to the outward and return path of the emitted pulses, the distance d $(in\ m)$ for one path should be multiplied by a factor of two, therefore:

$$S = 2d. \tag{1}$$

The speed of sound in air c_L can be calculated using the equation:

$$c_L = 331.3\ \frac{m}{s}\sqrt{1 + \frac{T}{273.15\ °C}}, \tag{2}$$

where the value of 331.3 m/s represents the speed of sound at 0 °C (273.15 K). The distance d between the source and target could then be easily calculated using the half of the measured t values, which could be detected at predefined distances and later compared to theoretical values obtained from the following equation to investigate the sensors' precisions:

$$t = \frac{S}{c_L} = \frac{2d}{331.3\frac{m}{s}\sqrt{1 + \frac{T}{273.15\ °C}}}, \tag{3}$$

or

$$d = \frac{t}{2}\ 331.3\frac{m}{s}\sqrt{1 + \frac{T}{273.15\ °C}}. \tag{4}$$

1.1 Investigation of the stability and the resolution of the digital signal output

1.1.1 Determination of the detection angle of the ultrasound sensors

Investigations aiming to determine the detection angle of the installed transducers are essential, especially in case of applying more than one sensor for a simultaneous distance measurement at more than one point. For this purpose, an ultrasonic sensor was placed at a fixed distance d_1 to a reflection object of hard cardboard (in this case: $d_1 = 50\,mm$), Fig. 4. This object contains a gap of width l, which could be enlarged uniformly and axially-symmetrical to the sensor. In this way, it was possible to define, to which gap size reflections take place. In order to avoid errors due to unwanted reflections, a second reflecting object made of cardboard was installed behind the gap at a fixed distance $d_2 = 500\,mm$. Since the distance between the sensor, the first reflection object and the corresponding gap size are known, the emission angle can be calculated using trigonometric functions and considering the half gap width h ($h = l/2$). With both sensors, measurements were applied using both sensors with h of 5, 10, 15, 20 and 21 mm. 1000 measuring time values were recorded for each h value. It was then investigated at which gap width unwanted reflections arise through the second reflection object. By exceeding a half gap width h of $20\,mm$, a strong extension of the measuring time of both sensors was recognizable. The resulting data suggest that even a marginal increase in the gap width leads to congruent sensor measuring times for both sensors. The calculation of the detection angle α was based on the following equation:

$$\alpha = 2arctan(\frac{h}{d_1}), \tag{5}$$

where $h = l/2$.

At a half gap width h of 21 mm, a total detection angle of 45.56° (22.78° for each side of the symmetry axis) was calculated. This result corresponds to previous experiments (see [13]), where most of the received signals are within a detection angle of 45° with only few outliers in the immediate vicinity of the sensors that occupy a larger detection angle. The detection area A of the sensor (green area in Fig. 4), which should be considered to prevent mutual influences of the sensors that work simultaneously, is dependent on the distance to the reflection object and can be calculated according to the following equation:

$$A = d_1 h\,. \tag{6}$$

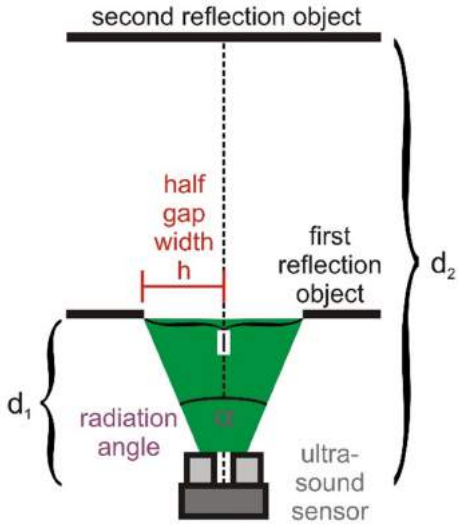

Fig. 4 Experimental setup for the determination of the detection angle of the ultrasound sensors HCSR04 and HYSRF05.

1.1.2 Influence of delay time value (delay time) on the stability of the measuring time

The measuring frequency for the applied measurements using an ultrasonic sensor should be set by defining delay time values between the individual measurements. For both sensors, manufacturers recommend a value between 50 and 60 ms ([14], [15]). Since the delay time is not sufficiently considered in the data sheets, it was assumed that the delay

time could be reduced at smaller distances. In order to study the best possible measuring quality that can be obtained from the used sensors, it was necessary to study this effect. For this purpose, a flat cardboard reflective object was positioned at a distance of $40\ mm$ away from each of the used sensors. Subsequently, three series of measurements were taken at the same distance with different delay time values (0.5 / 0.75 / 1 / 2 / 5 / 10 /20 / 40 / $60\ ms$). $1000\ t$ values were recorded for each fixed delay time value, from which a standard deviation was calculated. An average value was calculated from the resulting 27 standard deviations and the mean values of the calculated standard deviations were then studied in dependence of the set delay time values. The results showed a strong deviation of the recorded measured values when the delay was below a value of $1\ ms$. This indicates that decreasing the delay value below this limit to achieve a higher measuring frequency is not recommended.
Furthermore, the relationship between the calculated program run-times and the delay times was studied. The results showed a strong reduction in the program run-time when the delay was below a value of $1\ ms$. A comparison with the previous results suggests that the significant reduction in the program run-time affects the measuring stability of the sensors. At a reflecting object's distance of $40\ mm$, a delay time of $1\ ms$ results in a $2.121\ ms$ total average time difference between the successive measurements using the HCSR04 sensor (i.e. one measurement every $2.121\ ms$). This corresponds to a maximum measuring frequency of $471.52\ Hz$ for the sensor at this distance. The average time difference in case of using the HYSRF05 sensor is $2.083\ ms$, which corresponds to a measuring frequency of $480.13\ Hz$.

1.1.3 Approximate determination of the maximum distance between the sensor and the reflection object

In the following series of measurements, the linearity of the recorded measuring times at predefined distances from 200 to $3800\ mm$ was studied with an increment of $200\ mm$ and at a room temperature of $21.1\ °C$. With the given distances, measured with the help of a measuring gauge, and temperature values, the theoretical duration values of sound could be calculated according to equation 3. For each sensor, the results were compared with the measured time values at the corresponding distances with the help of the ultrasound sensors. For each predefined distance, the average value of 1000 digitally recorded time values and the standard deviation was calculated. A distinctly higher standard deviation should correspond to an unpresentable distance measurement.
Using the HCSR04, the standard deviation of the distance values calculated from the resulting measuring times (see equation 4) at the pre-adjusted distances from 200 to 800 mm had an average of 0.2 mm. At 1000 mm, a standard deviation of 2.93 mm was calculated, which was considerably higher than the calculated values at the former measurements. At 3600 mm, this value reached a standard deviation of 7.86 mm. The HYSRF05 showed a somewhat similar behaviour, with an average of standard deviations of 1.0 mm at pre-adjusted distances from 200 to 800 mm, while the standard deviation value at 1000 mm was 3.4 mm. This value increases gradually at larger distances to reach 7.24 mm at a predefined distance of 3800 mm. It was therefore concluded that, the maximum distance between the sensor and the reflection object should be significantly smaller than 1000 mm.

1.1.4 Approximate determination of the optimal distance between the sensor and the reflection object and the sensors' resolution

Preliminary ordinary experiments for the measurement of predefined distance changes with the help of the used ultrasound sensors had been performed by moving a cardboard wall on a scale ground at a sensor-object distance between 20 and $200\ mm$ with an increment of $10\ mm$. After averaging the resulting data and calculating the standard deviations at each predefined distance, the smallest deviations were found at distances between $40\ mm$ and $60\ mm$ using the HCSR04 sensor, while the most accurate results could be achieved using the HYSRF05 sensor at distances between $120\ mm$ and $140\ mm$. These distance ranges were used as a basis for subsequent precision experiments, for determining the finest possible sensors' resolution.
There are different documented values by different manufacturers for the resolution of the used ultrasonic sensors (varying between 2 and 4 mm). In order to determine the best possible actual resolution of the sensors, an experimental setup (see Fig. 5) had been used, with which even the smallest predefined distance changes could be realised. This setup should prevent runtime errors occurring, for example, due to small changes in the angle of the reflection object. Principally, the measurement of the distance between the circuit board and the reflecting object was performed. The front part including the transmitting and receiving units was not considered.

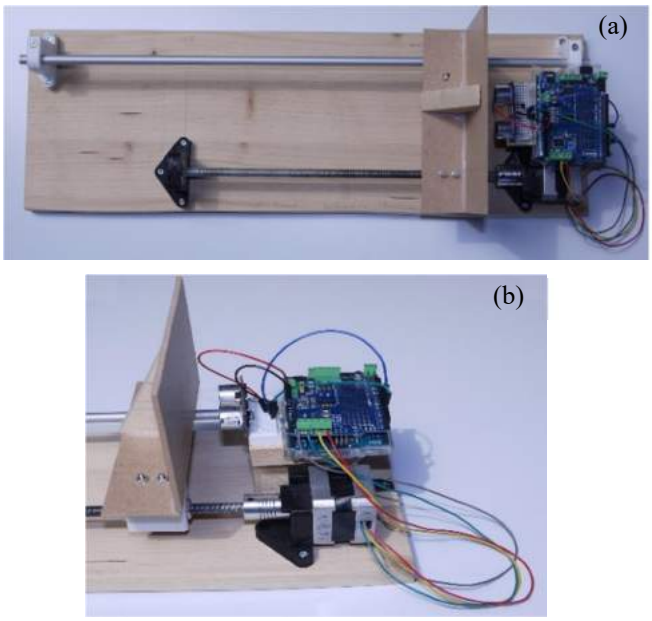

Fig. 5 Experimental setup for the determination of the optimal distance between the sensor and the reflection object. (a): top view of the spindle construction, (b): detailed view of the spindle assembly.

The setup consisted of a threaded rod (spindle) (M8 ISO threaded rod with a pitch p of $1.25\ mm$), which could be rotated by means of an electric motor (model: NEMA 14, with a full step angle of 1.8°) in very small, uniform steps. A wooden wall was mounted on the rod and could be used as a movable reflection object. To ensure the stability of this object, a guide rail was installed parallel to the rod, which was connected to the wooden wall by a linear bearing. The rod was attached by means of a shaft coupling to the step motor and is rotatably supported by a ball bearing on the opposite side. The fixations for the threaded rods and the guide rail were produced with the help of a 3D printer to be best adapted to the experimental setup. Since the used Arduino UNO could not supply the voltage required by the engine (12 V) and is also unable to handle higher electrical currents, a motor driver (model: Motorshield V2 from Adafruit) was installed. It was mounted directly on the Arduino UNO and can power up to two stepper motors simultaneously. Step angles of 0.9 ° could be realized by using the so-called interleave mode of the motor driver, in which alternates between one and two coils of the stepping motor could be performed. Using the step motor's half-step angle (mechanical play, input $\Delta\varphi_{in}$) and the pitch of the threaded rod p, the driven distance Δs_l (mechanical play, output) could be calculated using the following equation [16]:

$$\Delta s_l = p\frac{\Delta\varphi_{in}}{360°}, \tag{7}$$

which allowed a smallest possible distance change of $0.003125\ mm$ at a step angle of $0.9°$.
Two precision distance measurements (using each of the two ultrasound sensors. Each measurement was repeated three times for the statistical analysis) were performed using the above-mentioned setup to determine the finest possible resolution which could be obtained from the digital signal output. The predefined sensor-object distance changes were carried out at distances between 40 and $60\ mm$ using the HCSR04 sensor and between 120 and 140 mm using the HYSRF05 sensor with a $0.1\ mm$ increment.
1000 values were recorded per distance and the mean values and standard deviations were calculated. The relationship between the actual real distance and the mean values of the measured time at each distance was then plotted for each measurement. In addition to the expected linear increase, some deviations were detected in terms of peaks using both sensors (see Fig 6).

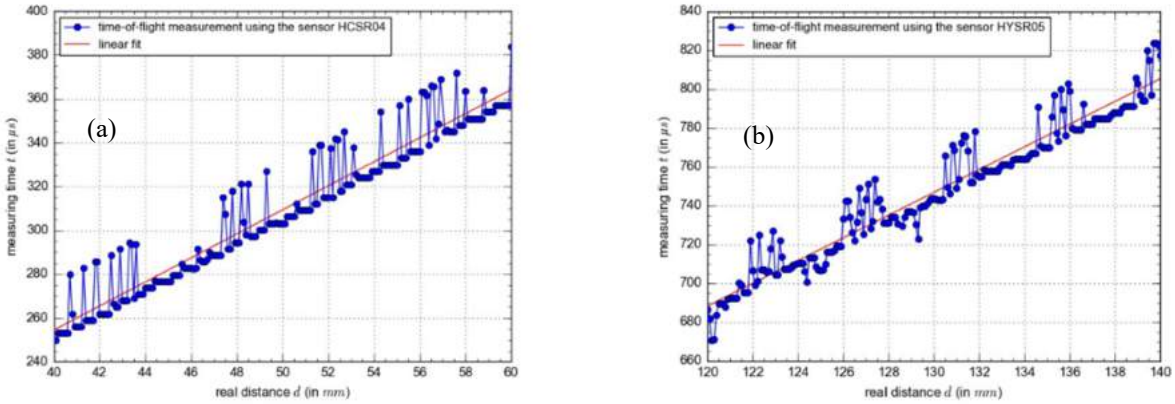

Fig. 6 Relationship between the real pre-defined distance d and the measuring time t using the HCSR04 (a) and the HYSRF05 (b) sensors.

The peaks that represented a kind of outliers with respect to linear characteristic of the relationship between the real distance change and the measured time value, were then filtered out (for more details about the filtering method, see [8], chapter 15.1). After filtering the data, the plots showed a distinct step characteristic in addition to the general linear increase of the measuring time with respect to the increase of the real distance. This characteristic was then specifically analysed, since the number of steps N (here: $N = \frac{0.1\ mm}{0.003125\ mm} = 32$) in relation to the considered distance range ($d_r = 20\ mm$) corresponds to the theoretical digital resolution R of the sensor (see [17]) according to the following equation:

$$R = \frac{d_r}{N}, \tag{8}$$

where R was $0.625\ mm$.
The calculated average resolution of the sensor HCSR04 at distances between $40\ mm$ and $60\ mm$ was $0.58\ mm$, and the average resolution of the sensor HYSRF05 at distances between $120\ mm$ and $140\ mm$ was $0.53\ mm$.

1.1.5 Investigation of the measuring time stability

Taking the results in chapter 1.1.4 (Fig. 6) into consideration, a calculation was performed at the same distance ranges to investigate the measuring time stability of both sensors. The results of this investigation should show, how strong the output data (t-values) deviate, when performing continuous measurements at a constant distance. The standard deviation of the resulting $t-$values at each predefined distance and the mean value of all the calculated standard deviations at each distance within the whole distance range were calculated. These calculations were performed three times for three successive measurements for each sensor. The mean value of the three results gave out an average standard deviation of $1{,}89\ \mu s$ for the HCSR04 and $2{,}78\ \mu s$ for HYSR05 sensor, which shows a higher measuring time stability for the HCSR04 than for the HYSR05.

1.1.6 Investigation of the highest measurable frequency

Different methods had been used during this project to define the maximum frequency with which a flat surface of an object oscillates, and still can be detected by the used ultrasonic sensors. According to the Nyquist theorem, the sampling rate of the sensor must be set to be at least twice as high as the signal to be detected [18]. Referring to the results in Chapter 1.1.1, delay times of minimum $1\ ms$ were adjusted. To determine the measuring frequencies, the digital measuring times of both sensors were investigated and plotted over a period of one second. The frequency detected by the sensors was then determined from the number of peaks and valleys of an oscillating reflection object. The mechanical excitation of the reflection object was applied in three different ways: a) Using an Arduino controlled solenoid magnet which generates a linear motion of an attached metal pin due to the mutual activation and deactivation of an induced magnetic field, and a motor driver. The maximum frequency that could be generated using this method was about $14\ Hz$ due to the limited magnetic force which was after $30\ ms$ insufficient to completely deflect the metal pin. b) Using an oscillating speaker cone with a plastic disk being glued on its outer membrane, and a frequency modulator software to generate frequencies in the range from 20 to $20000\ Hz$. The mechanical deflection of the surface of the disk could not be detected at frequencies over $80\ Hz$, due to the decrease of the signal amplitude with increasing the excitation frequency. c) Using a permanent magnet driven shaker with a metal pin (similar to a)) which simulated the vibration condition of a styrofoam wall (reflection object), and a frequency generator. The wall had the dimensions of

$50\ mm * 75\ mm * 5\ mm$ and was installed on the surface of the pin with the help of a screw connection. Much higher frequencies than in the last two methods could be generated using this setup, therefore the experiments were performed with the help of the above-mentioned shaker. The measurements were applied using the HCSR04 sensor at a zero position of $54\ mm$ from the reflection object, and at $120\ mm$ using the HYSR05 sensor. The frequency was increased in uniform steps with the help of the frequency generator. The measurements have shown that the maximum detectable frequency of both sensors is $110\ Hz$. At higher frequencies, the noise components increased strongly, and thus prevented accurate identification of the actual number of oscillations.

1.2 Investigation of the stability and the resolution of the analogue signal output

Using the mentioned ultrasound sensors to detect mechanical displacements on solid surfaces is not widely used due to, for example, resolution and stability limitations. Closer investigations had been made (see last chapters) to define the best possible resolution values, that could be obtained from reading the digitally processed values by the sensors. The aim of this study is to test the possibility of obtaining a better resolution using the analogue output of each of the sensors. For the first investigations, the experimental setup shown in Fig. 5 as well as the determined maximum and optimal distances between the sensor and the reflecting object using the digital signal output were taken into consideration. This means that the experiments in this section were carried out at distances between 40 and 60 mm using the HCSRF04 sensor and at distances between 120 and 140 mm using the HYSRF05 sensor. The reflection object had been moved horizontally with a distance increment of 0.1 mm. The room temperature had been measured simultaneously and was considered in the calculations. The voltage output was recorded with the help of a digital oscilloscope which contains 2 channels (channel: CH). The output signal of each of the used sensors was recorded from CH1 and CH2 with a sampling rate of 1 MHz and included 10 distance measurements per pre-defined distance (200 positions). The sensors' analogue output of the echo pin is a square wave and was recorded by one of the channels (CH1). The time duration of a step corresponds to the measuring time t obtained from the digital output. The second channel (CH2) was used parallel to record the voltage output, which was detected at the receiver unit of the HCSR04 or at the collector of the BC857 PNP transistor of the HYSRF05 sensor. Unlike the echo's square wave, the voltage signals of the sensors show different behaviours (see Fig. 7). The envelope of the analogue output signal of the HCSR04 sensor showed a Gaussian-like behaviour with one or more global maxima and minima, whose amplitude varied by changing the distance to the reflection object. The signal could be amplified and smoothed (filtered) with the help of the 4x operation amplifier (type: LM324) and showed uniformly arranged peaks of amplitudes fluctuating between 4.5 and 5 V.

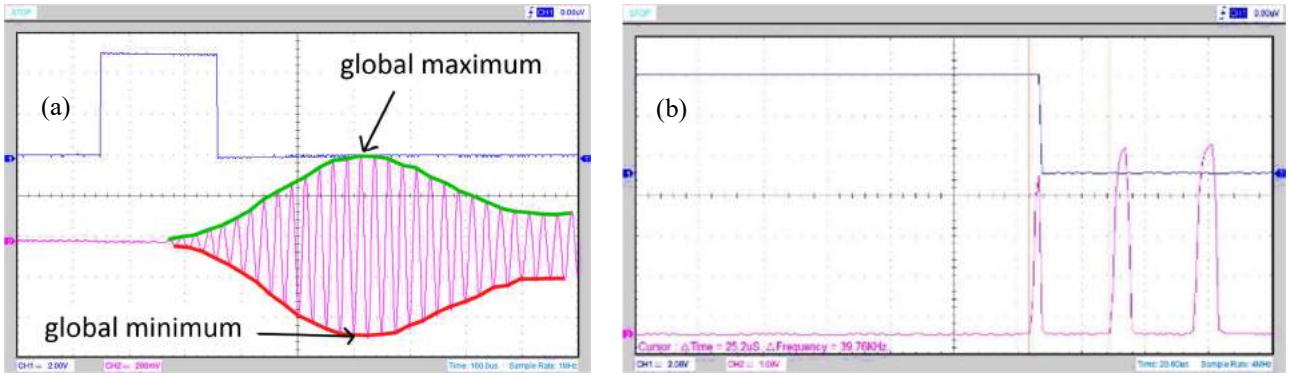

Fig. 7 Voltage signal output of the HCSR04 (a) and the HYSRF05 (b).

1.2.1 Investigation of the measuring time stability of the analogue signal

The analogue voltage signal resulting from the distance measurement using an ultrasound sensor was processed and investigated using a LabVIEW program code (individually written for each sensor). The output signals of both channels were analysed to detect any sensor-specific characteristic which behaviour correlates to the variation in the distance between the sensor and the reflection object. As mentioned before, the recorded signal at CH2 using the HCSRF04 sensor has a different behaviour than the recorded one using the HYSRF05 sensor. Therefore, the signal processing method differ from one sensor to the other.

For this investigation, the signal was subdivided into 10 sections (1 section per measurement at a constant distance, see Fig. 8). The definition of a section was based on the time intervals between the detected echo signals' starts (the time-points of the left flanks of the square wave).

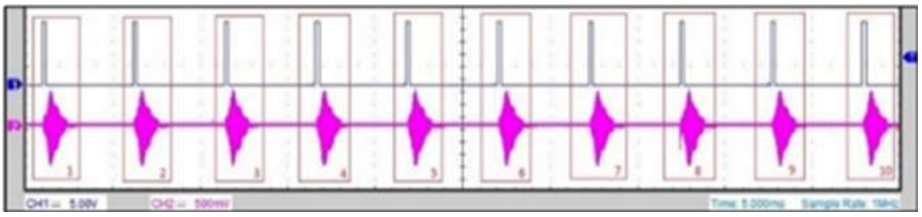

Fig. 8 Representation of the output signal's division into 10 sections representing the individual measurements (used sensor: HCSR04).

Fig. 9 represents the program which was used for determining the measuring time stability of the analogue data generated by the HCSR04 sensor while moving a reflection object at distances between 40 and 60 mm with an increment of 0.1 mm using the setup in Figure 5. The fact that the time position of the global maximum/minimum of the sensor's output signal in one section changes by changing the distance of the reflection object, has been the base of further calculations. The program consists of two main paths; each path being assigned to a channel of the oscilloscope. The first channel detects the time duration of the recorded echo signal of each measurement section. The mean and standard deviation of the measuring times at each distance were then calculated from the 10 sections. In the next step, the calculated standard deviations of the individual distances are averaged and thus the stability value of the first channel is determined.

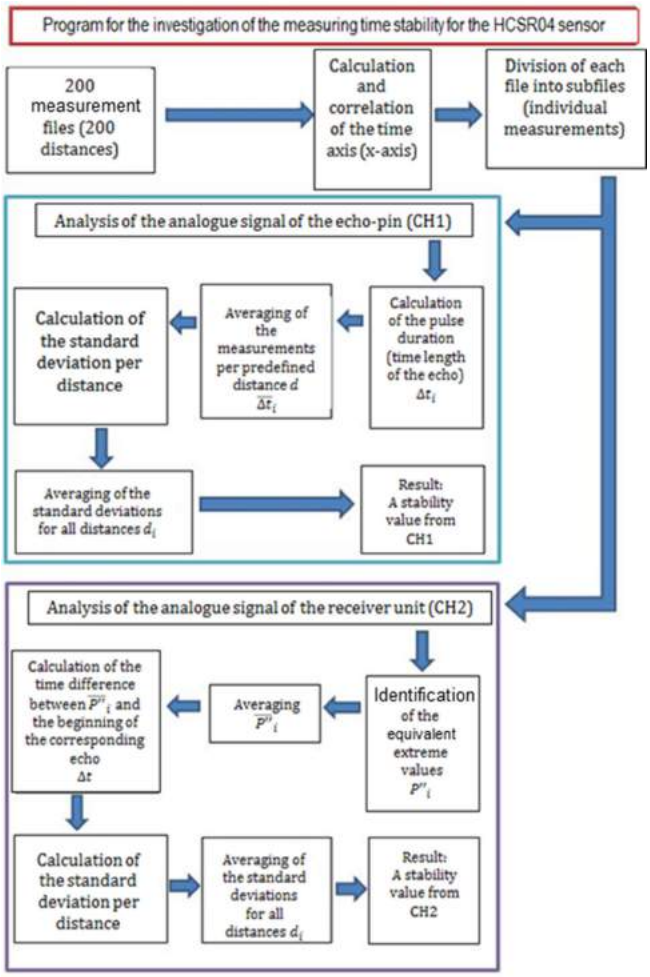

Fig. 9 Program plan for the processing of the analogue output signal of the sensor HCSR04.

Fig. 10 represents the plan of the LabVIEW program used for the processing of the analogue output signal of the HYSRF05 sensor. The processing of the CH1 signal is identical to that used for the HCSR04, while the signal processing of CH2 is different. Instead of considering the time position of the maxima/minima at different distances, the first peak was used as a reference. The calculation of the stability value was done using the standard deviation value at each signal section (constant distance) and the average of all standard deviation values at each of the 200 pre-defined distances.

The calculations for the HCSR04 sensor resulted in an average standard deviation of $5.09\ \mu s$ for the signal of CH1 and $20.79\ \mu s$ for the signal of CH2, and those for the HYSRF05 sensor resulted in an average standard deviation of $19.85\ \mu s$ and $17.59\ \mu s$ for the Signal of CH1 and CH2 respectively. The stability of the recorded signal at CH1 corresponds to the stability of the digital signal due to the identical method of the measuring time calculation which is later used for the calculation of the distance to the reflection object. This signal showed more stability using the HCSR04 sensor. On the other hand, the stability of the recorded signal at CH2 showed more stability using the HYSRF05 sensor. An investigation of the resolution which can be obtained from the analogue signal is still necessary for the selection of the adequate sensor for the intended application.

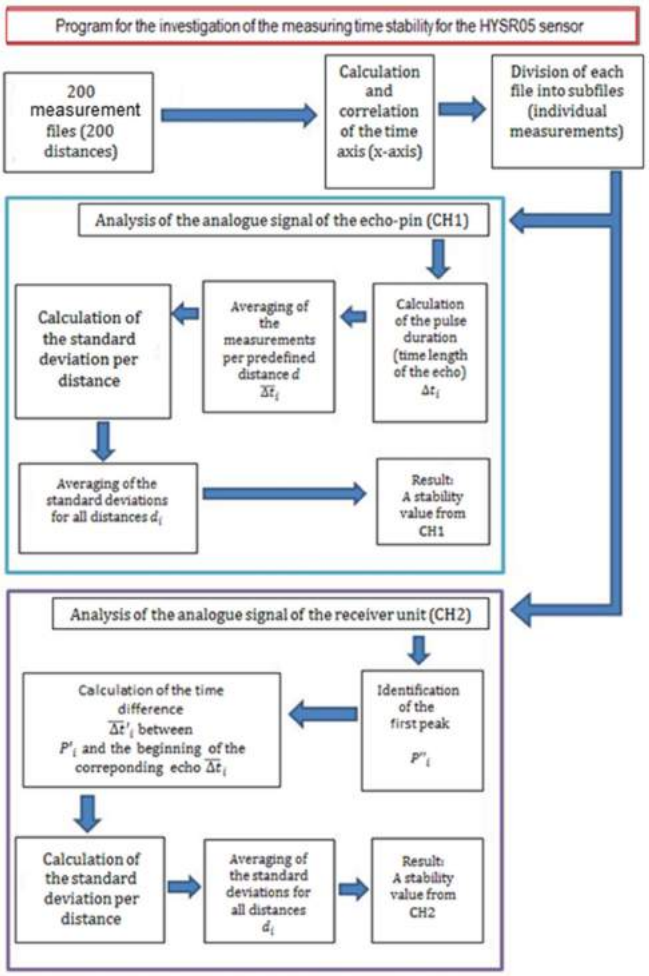

Fig. 10 Program plan for the processing of the analogue output signal of the sensor HYSRF05.

1.2.2 Investigation of the resolution of the analogue signal

The investigation was based on the relationship between the real distance which was pre-set using the setup shown in Fig. 5, and the average measuring time value calculated from the recorded analogue signal (CH1 and CH2) by the ultrasonic sensor at the corresponding position.

The results of CH1 are comparable to the results of the digital signal output discussed in the last chapter. The plot shown in Fig. 11 (left) shows a step characteristic in addition to the general linear increase of the measuring time with respect to the increase of the real distance. This was to be expected, since the procedure for determining the measuring time here is identical to that of the microcontroller. The evaluation of the measured values yielded therefore a resolution of approximately $0.58\ mm$ for the first channel. The resulting curve from CH2 showed a completely different characteristic. Instead of an expected uniform linear increase, a linearly increasing sinusoidal-like curve is recognizable (see Fig.11, right). For this reason, no further signal processing was performed, as the amplitude of the curve decreases regularly at multiple positions and then rises until it reaches a peak level, then decreases again. This makes a correlation to the regularly increasing real distance unfeasible.

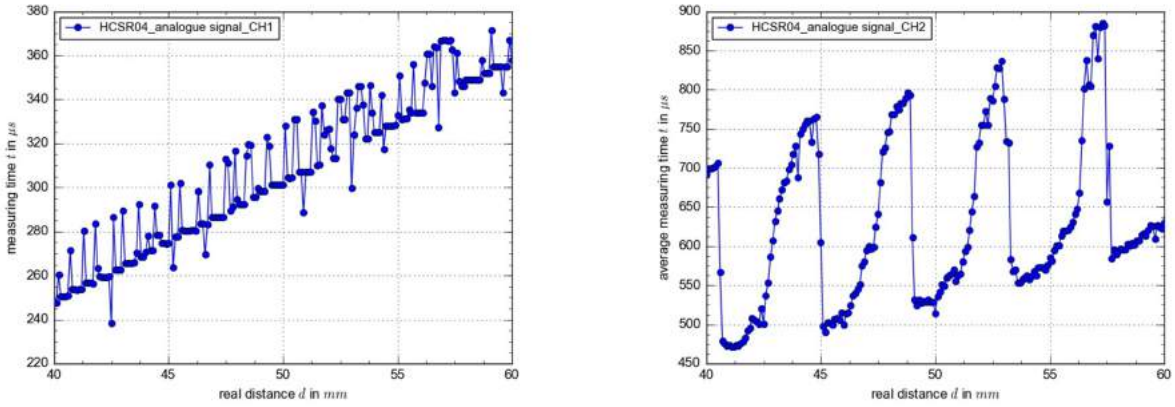

Fig. 11 Relationship between the measuring time and the real distance using the recorded analogue signal at CH1 (left) and CH2 (right). Sensor: HCSR04.

In the next step, and with the help of the same setup and exchanging the ultrasonic sensor, the feasibility of using the analogue signal output of the HYSR05 sensor was investigated. With a real distance increment of $0.1\ mm$, an expected curve behaviour had been established at CH2 as well as CH1 (see Fig. 12). However, instead of a step characteristic accompanying a general linear increase of the curve, the signal output of CH2 shows a steady linear increase in the curve amplitude with multiple valleys (noise). This motivated further signal processing for the analogue output of CH2.

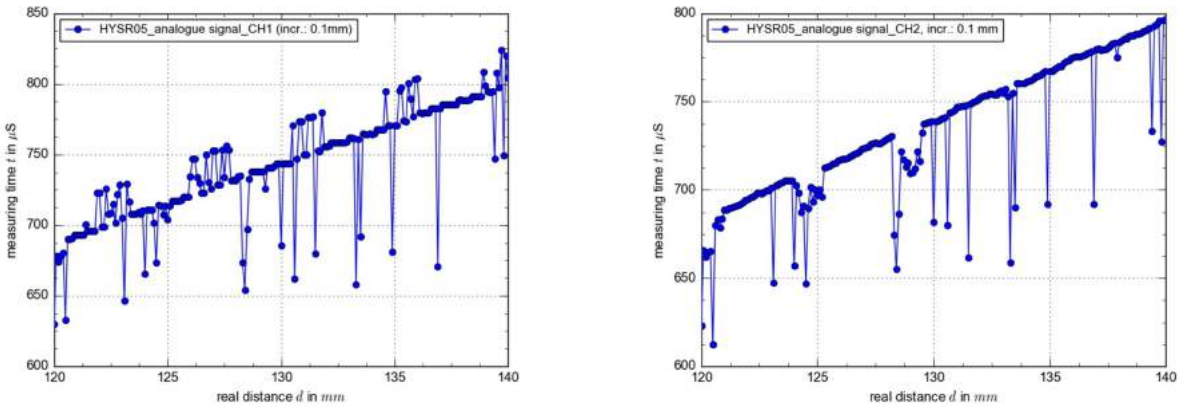

Fig. 12 Relationship between the measuring time and the real distance using the recorded analogue signal at CH1 (left) and CH2 (right). Sensor: HYSRF05, distance range: $120 - 140$ mm, increment: 0.1 mm.

The signal portion with the least background noise and a permanent positive slope had been programmatically selected and was taken as a basis for subsequent measurements with smaller distance increments ($0.075\ mm$, $0.05\ mm$ and $0.0125\ mm$). The distance range between $135\ mm$ and $136\ mm$ was chosen for these experiments to try to approach the maximum resolution of the sensor. The results of the experiment using a distance increment of $0.0125\ mm$ are shown in Fig. 13.

The measurements were then analysed using a special program which includes two filters to determine the maximum resolution in this distance range. The first filter allowed only signal portions of a slope greater than or equal to zero, and the second filter is based on the comparison between the slope of this filtered signal and that of the theoretical curve (the relationship between the real distance and the calculated measuring time values using equation 1). A maximum resolution of $0.0125\ mm$ could be determined at a distance range between 135 and $136\ mm$. This result shows that the analogue output signal of the HYSRF05 sensor has a potential for applications concerning the detection of very small displacements and might be suitable for the detection of structural vibrations.

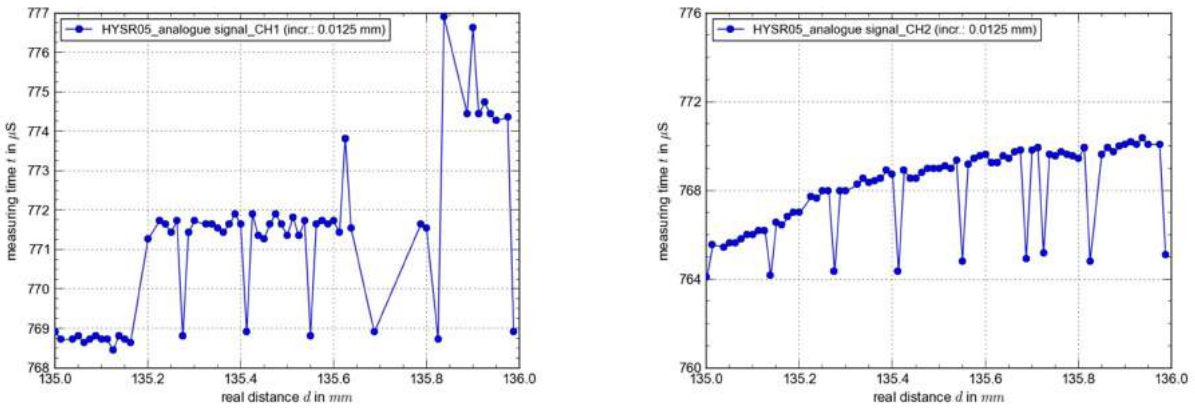

Fig. 13 Relationship between the measuring time and the real distance using the recorded analogue signal at CH1 (left) and CH2 (right). Sensor: HYSRF05, distance range: $135 - 136$ mm, increment: 0.0125 mm.

2 Summary and outlook

The aim of this project is the investigation of the feasibility of two inexpensive types of ultrasonic sensors for measuring the mechanical deflection on vibrating surfaces. For this purpose, the sensors were tested extensively regarding to their measuring time stability, the maximum detectable frequency as well as the distance resolution. The digital and the analogue signal outputs were evaluated, and the following results have been obtained: The measuring time stability of both sensors is strongly dependent on the delay time between the individual measurements. If it goes below $1\ ms$, the software of the microcontroller cannot completely execute its arithmetic operations. This results in runtime errors, which are slightly lower when using the HCSR04 sensor than when the HYSRF05 is used. Based on these results, multiple experiments were performed to determine the sensors' maximum detectable frequencies with a pre-adjusted delay of $1\ ms$. Both sensors delivered reliable distance values (measuring time values) at a maximum frequency of $110\ Hz$. After defining the optimal measuring distance between the ultrasonic sensors and the reflecting object, the resolutions of the digital and the analogue signal output of both sensors were then investigated. The resolution of the digital signal output of the HYSRF05 sensor ($\sim 0.53\ mm$) was higher than that of the HCSR04 sensor ($\sim 0.58\ mm$). The analogue signals of both sensors showed significant differences due to the selection of different ports to read the analogue voltages. The voltage output of the HCSR04 sensor was not further processed, because its behaviour was inconsistent with the expected linear behaviour over a uniform increase in distance between the sensor and the reflection object. Unlike the voltage output of the HCSR04, the HYSRF05 sensor showed an approximate linear increase in the voltage value by increasing the distance to the sensor, with the exception of some background noise (peaks). A maximum resolution of $0.0125\ mm$ could be determined using the HYSRF05 sensor at a distance change range between 135 and $136\ mm$. The differences between the digital and analogue resolutions might have been occurred due the microprocessor's used polling method by both sensors (see [8]). This method leads to the regular detection of incorrect measuring values during the peak detection of digital signals, since very short voltage variations were frequently not recorded. Therefore, the digital signal output is not appropriate for the detection of small surface displacements, and the processing of the analogue signal output might be the best possible solution for this application using the mentioned ultrasonic sensors.
Future experiments should be realized using a setup that consists of 64 ultrasonic sensors of the type HSRYF05. The goal of these experiments is a synchronous contact-free surface displacement measurement at 64 points to generate a kind of a real-time vibration pattern for a vibrating rectangular surface. Due to the fact that a microcontroller allows only single core processing, a parallel programming of multiple ultrasonic sensors cannot be performed using an Arduino board. However, an almost simultaneous recording of the output data could be realized by improving the programming code, for example with the help of the so-called protothreading [19]. Therefore, further future studies should include the improvement of the Arduino's microcontroller's software or the replacement of the Arduino board with a multi core programmable computer, such as Raspberry Pi [20] which should allow a parallel connection between multiple ultrasonic sensors for a simultaneous distance measurement at each of the 64 points. Moreover, extensive investigations should be performed to study the possibility of a sufficient isolation of individual ultrasonic signals that travel from and back to each of the sensors to prevent erroneous measurements. The following figure shows a schematic arrangement of 64 ultrasonic sensors for the measurement of distance changes on the surface of a reflection object (blue rectangle) and the radiation lobes of the individual sensors.

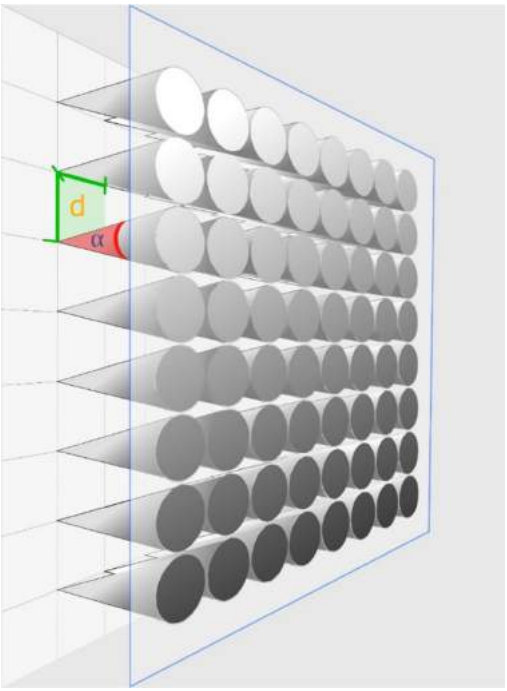

Fig. 14 Overview of the ultrasonic sensors' arrangement. α: detection angle, d: distance between the individual sensors.

3 Literature

[1] Germanischer Lloyd Aktiengesellschaft: Rules for Classification and Construction, I Ship technology: ch. 23, 2009, p. 1.

[2] Asmussen, I., Menzel, W., Mumm H.: Ship Vibration. GL Technology, 2001, p. 7.

[3] Göken, J., Fayed, S.: A Report on Different Vibration Analyses Based on Acoustic and Mechanical Measurements. Schriftenreihe der Hochschule Emden/Leer, Bd. 23, Emden, Germany, 2017, ISBN: 978-3-944262-13-0.

[4] Göken, J., Ahrends, H., Brink, H.: Use of a Sound Source Localisation System for the Experimental Determination of the Vibration Patterns of a Square Plate. ARPN JEAS, 9 (10), 1983-1993 (2014).

[5] Parallax Inc., [Online]. Available: www.parallax.com. [Accessed 5 May 2018].

[6] Emil's Projects: OpenHardware & OpenSource: Making a Better HC-SR04 Echo Locator, 22 January 2014. [Online]. Available: www.uglyduck.vajn.icu/ep/archive/2014/01/Making_a_better_HC_SR04_Echo_Locator.html. [Accessed 23 January 2018].

[7] E. M. Corporation: EM78P152/3S Product Specification, April 2016. [Online]. Available: http://www.emc.com.tw/chs/database/Data_Sheet/8BIT/EM78P153S.pdf. [Accessed 26 May 2018].

[8] Bomhoff, L.: Erstellung eines experimentellen Versuchsaufbaus zur flächenhaften Messung von Distanzänderungen mittels Ultraschallsensoren, Laboratory of Materials Physics: University of Applied Sciences Emden/Leer, 2018 (bachelor thesis).

[9] Arduino Uno Rev3, Arduino, 2018. [Online]. Available: www.arduino.cc. [Accessed 15 June 2018].

[10] Caroli, P., Caroli C.: Arduino Handbuch: Platinen, Shields, Elektronik and Programmieren: mehr als 20 Projekte als Startpunkt für eigene Vorhaben, Haar: Franzis Verlag, 2015.

[11] "Python," Python Software Foundation, [Online]. Available: www.python.org. [Accessed 15 June 2018].

[12] Kurzweil, P., Frenzel, B., Gebhard F.: Physik Formelsammlung: Für Ingenieure und Naturwissenschaftler. Wiesbaden: Vieweg + Teubner Verlag, 2008.

[13] „Ultraschallsensor SRF05 für Entferunungsmessungen," Mikrocontroller-Elektronik.de, [Online]. Available: www.mikrocontroller-elektronik.de. [Accessed 27 May 2018].

[14] ELECFREAKS, „Ultrasonic Ranging Module HC - SR04," [Online]. Available: www.cdn.sparkfun.com/datasheets/Sensors/Proximity/HCSR04.pdf. [Accessed 2 February 2018].

[15] M. P. J. &. A. Inc., „HC-SR04 UserGuide," [Online].Available: www.mpja.com/download/hc-sr04_ultrasonic_module_user_guidejohn.pdf. [Accessed 28 December 2017].

[16] Braun, J., „maxon academy: Formelsammlung,“ 2012. [Online]. Available: https://www.maxonmotor.de/medias. [Accessed 22 February 2018].
[17] Lang, K.: Auflösung ist nicht gleich Genauigkeit. Elektronik Industrie, p. 73, 2002.
[18] Evans, D.H., McDicken, W.N.: Doppler Ultrasound: Physics, Instrumentation and Signal Processing, West Sussex, England: Wiley, 2000.
[19] ”How to "Multithread" an Arduino (Protothreading Tutorial) © GPL3+,“ Arduino, [Online]. Available: https://create.arduino.cc/projecthub/reanimationxp/how-to-multithread-an-arduino-protothreading-tutorial-dd2c37. [Accessed 7 May 2019].
[20] “Raspberry Pi,“ [Online]. Available: www.raspberrypi.org. [Accessed 7 May 2019].

Investigation of the Sound Pressure Distribution on Different Woods

Prof. Dr. rer. nat. habil. Jürgen Göken[1], M.Sc. Sarah Fayed[1], Herbert Otte[2]

[1] University of Applied Sciences Emden-Leer, Faculty of Maritime Sciences, Bergmannstraße 36, 26789 Leer, Germany
[2] Herbert Otte Furniere - Hölzer, Wiesenweg 2b, 26639 Wiesmoor, Germany

E-mail: juergen.goeken@hs-emden-leer.de; sarah.fayed@hs-emden-leer.de

Based on the fact, that wood is a natural construction material which has many advantages over other materials due to its high strength with good elasticity, high resistance against load levels, corrosion resistance in saline water, good workability, low costs and its outstanding environmental friendliness [1], it has become an important technical material for structural components in many industries, such as the automotive and shipbuilding industries as well as in musical instruments construction.

Due to poor forest management, illegal logging tends to be associated by environmental impacts including the loss or degradation of forests. This can result, for example, in the loss of habitats and biodiversity [2]. Deforestation and forest degradation also has implications for climate change, as forests have a crucial role in both mitigating against and adapting to climate change. Illegal logging in nine forest producer countries is estimated to have released 190 million tonnes of carbon dioxide into the atmosphere in 2013 [3].

Due to the rising importance of a sustainable management of wood supply from forests, new constraints prescribe a reduction, or even a prohibition of the trade of definite species of forest products with high yields. The highest yields are generally found in South America, followed by Asia and Africa [4]. For this reason, the interest in using native forest trees from Europe, like spruce and maple, in many technical applications has been growing faster over the past few years, and on this account, the importance of studying the mechanical and acoustic behaviour of these woods.

Previous measurements

In own preliminary studies, acoustic experiments on a double bass were performed in order to demonstrate the change of the sound distribution on the top plate after a slight alteration of the mechanical load on the bridge. The sound distribution was determined by measuring the local sound pressure level using a sound source localisation system. The comparison between both cases (before and after the alteration of the mechanical load) shows that already a slight alteration of the external mechanical load can lead to significant changes of the sound distribution. This illustrates the problem with regard to vibration analysis of musical instruments [5]. The vibration analysis of an oscillating plate is known to be very difficult. Exact mathematical solutions of the differential equation for a vibrating plate are extremely rare because the individual boundary conditions have to be met. For this reason, former work was targeted on the visualisation of the vibration behaviour of a clamped square plate using a sensitive sound localisation system which measured the local particle velocity of an oscillating acrylic glass pane. Further details can be found in the work of Göken et al. [6]. The comparison with the sand figures on the vibrating plates representing the Chladni figures showed that the highest particle velocity occurred in the center of the pane where hammering of a lifting magnet took place (position of exciting force). Firstly, the edges of the pane were clamped homogeneously. When four bar clamps were removed, the vibration pattern was not anymore as dendritic as before. The demounting of some bar clamps appeared to be sufficient to change the vibrating structure significantly. The results of the acoustic measurements clearly suggest that a musical instrument like a piano or a guitar represents a complex construction. Due to the mounting of different parts with individual vibration behaviours, a prediction of the overall sound experience is almost impossible. Therefore, measurements on individual parts and their mechanical properties are the driving forces for the optimisation of the acoustic design. These properties must be properly considered in order to make at least a rough estimation of the sound characteristics, which has been the topic of own extensive studies on the damping behaviour of the tonewood spruce. In this study, frequency, strain and moisture content dependent damping measurements had been performed on new and on 130-years old spruce wood, which is used in the manufacture of musical instruments. For more information about the experimental details and results, see [5].

This work

In cooperation with an experienced wood provider who is specialized in trading particularly exclusive woods for, among other applications, the musical instruments industry, experimental acoustic measurements have been performed with the help of frequency dependent external excitation of 14 relevant wood sheets to measure the resulting sound pressure distribution on their surfaces using a p-u acoustic probe accompanied by a digital camera. These measurements serve as a first indication for the acoustic practicability of exchanging commonly used woods in the manufactory of musical instruments like African white wood (Abachi) or South American rosewood (Santos) with other wood types produced in Europe, like cherry and spruce woods.

1 Experimental details

The experimental setup for this study (see Fig. 1) consists of a wooden frame which was used for the stable hanging of the sheets with the help of lightweight nylon cords, that drew each sheet at 8 points on the frame using equally twisted screw hooks. Furthermore, the setup comprises a frequency generator which controlled an electrodynamic shaker of a frequency range from 2 to 20000 Hz and a nominal force of 18 N, a p-u sound probe which was used to measure the resulting sound pressure changes on the surface of the wood sheets and a digital camera of which picture was correlated with the positions and the values of the measured sound pressure using the corresponding software. A piece of thick cloth was hanged around the sheets of wood, for less acoustical disturbance during the excitation. The expected results' character was a colour-coded sound pressure distribution on the surface of each sheet.

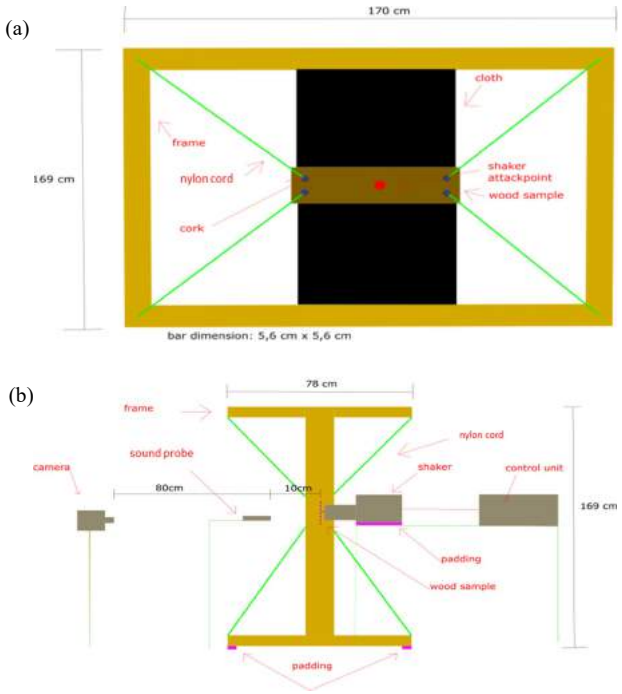

Fig. 1 Experimental setup: Measurement of the sound intensity distribution on a vibrating wooden sheet. (a): front view, (b): side view.

Two output signals from the p-u probe which incorporates a combination of a pressure transducer and a particle velocity transducer are multiplied together to give the time-dependent component of sound intensity in the direction of the probe axis [7]. On account of this, the sound intensity I is directly related to sound pressure p in an acoustic free field according to the equation:

$$I = pu\,, \tag{1}$$

where u represents the acoustic particle velocity. The resulting sound intensity value (in dB(A)) on each vibrating sheet had been recorded at 14 positions on the surface of the sheet, at 5 different exciting frequencies from the sound spectrum of a common acoustic guitar: 82.4 Hz, 146.8 Hz, 220 Hz, 440 Hz, and 659.3 Hz. A total of 14 wood sheets of different types and origins was investigated. The investigated timber included: European spruce, oak latch, maple latch and cherry, American maple and cherry, African Khaya, Padouk, Wenge and Abachi, South American Santos rosewood and Ziricote, as well as twisted and untwisted Acacia. The sheets have the dimensions of $505 \pm 1\,mm \times 148 \pm 1\,mm \times 1{,}5 \pm 0.06\,mm$, and were all investigated at room temperature.

2 Results

The resulting colour-coded sound pressure distributions on the wood sheets at 14 measuring points and at the predefined excitation frequencies of 82.4 Hz and 659.3 Hz are shown in the following images.

2.1 Exciting frequency: 82.4 Hz

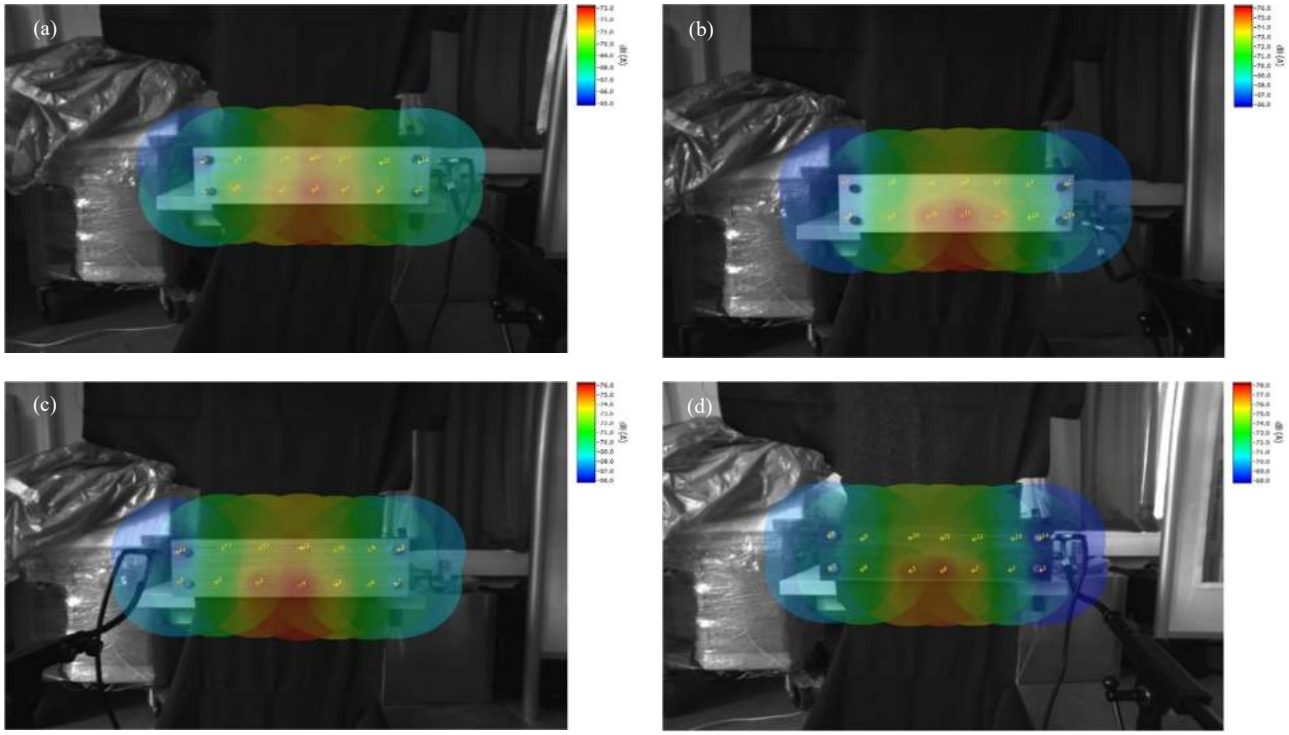

Fig. 2 Sound intensity distributions on wood sheets of European origin: (a) spruce, (b) maple latch, (c) oak latch, (d) cherry. Exciting frequency: 82.4 Hz.

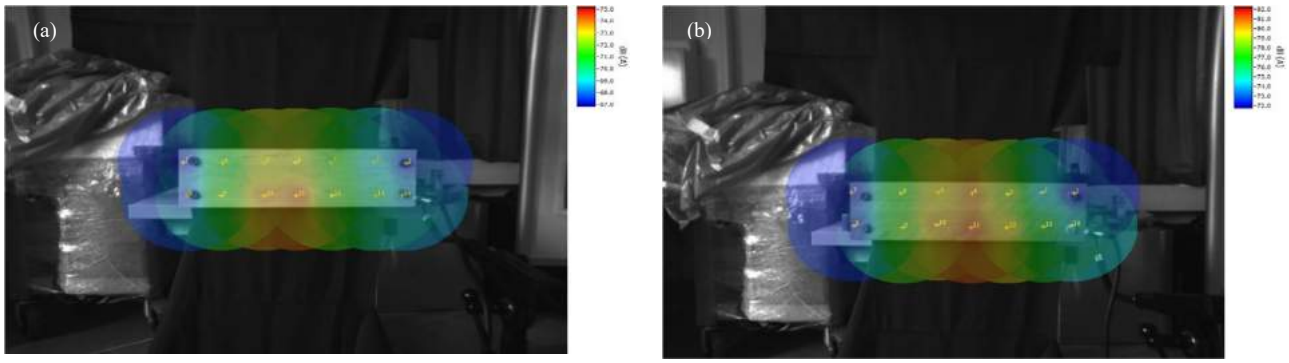

Fig. 3 Sound intensity distributions on wood sheets of American origin: (a) maple, (b) cherry. Exciting frequency: 82.4 Hz.

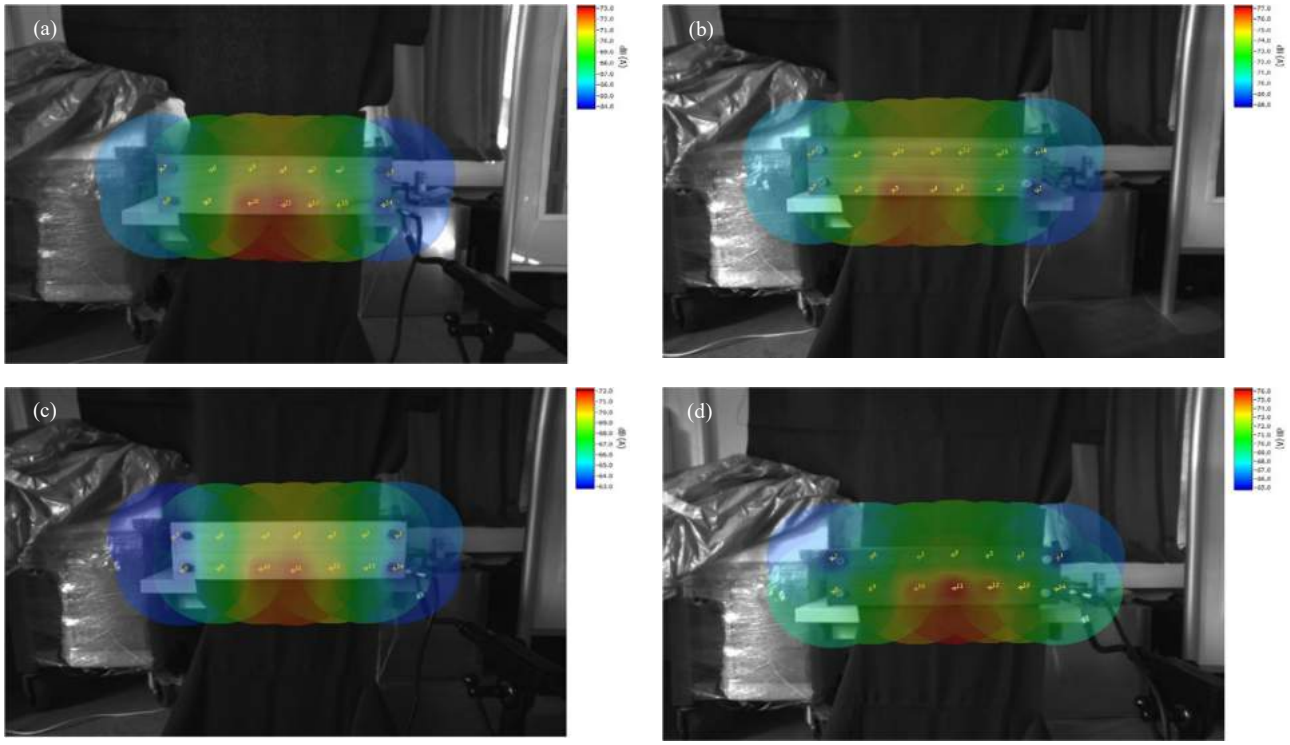

Fig. 4 Sound intensity distributions on wood sheets of African origin: (a) Khaya, (b) Padouk, (c) Abachi, (d) Wenge. Exciting frequency: 82.4 Hz.

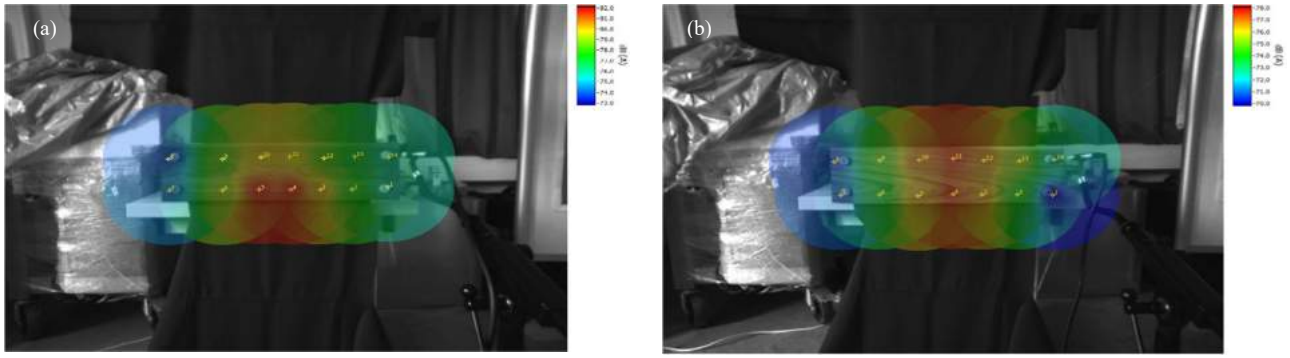

Fig. 5 Sound intensity distributions on wood sheets of South American origin: (a) Santos rosewood, (b) Ziricote. Exciting frequency: 82.4 Hz.

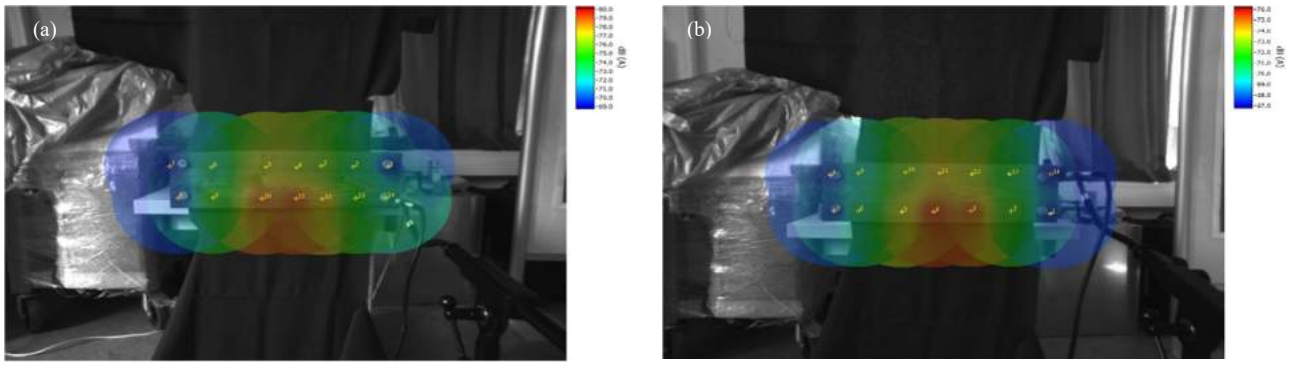

Fig. 6 Sound intensity distributions on wood sheets: (a) twisted, (b) untwisted Acacia. Exciting frequency: 82.4 Hz.

2.2 Exciting frequency: 659.3 Hz

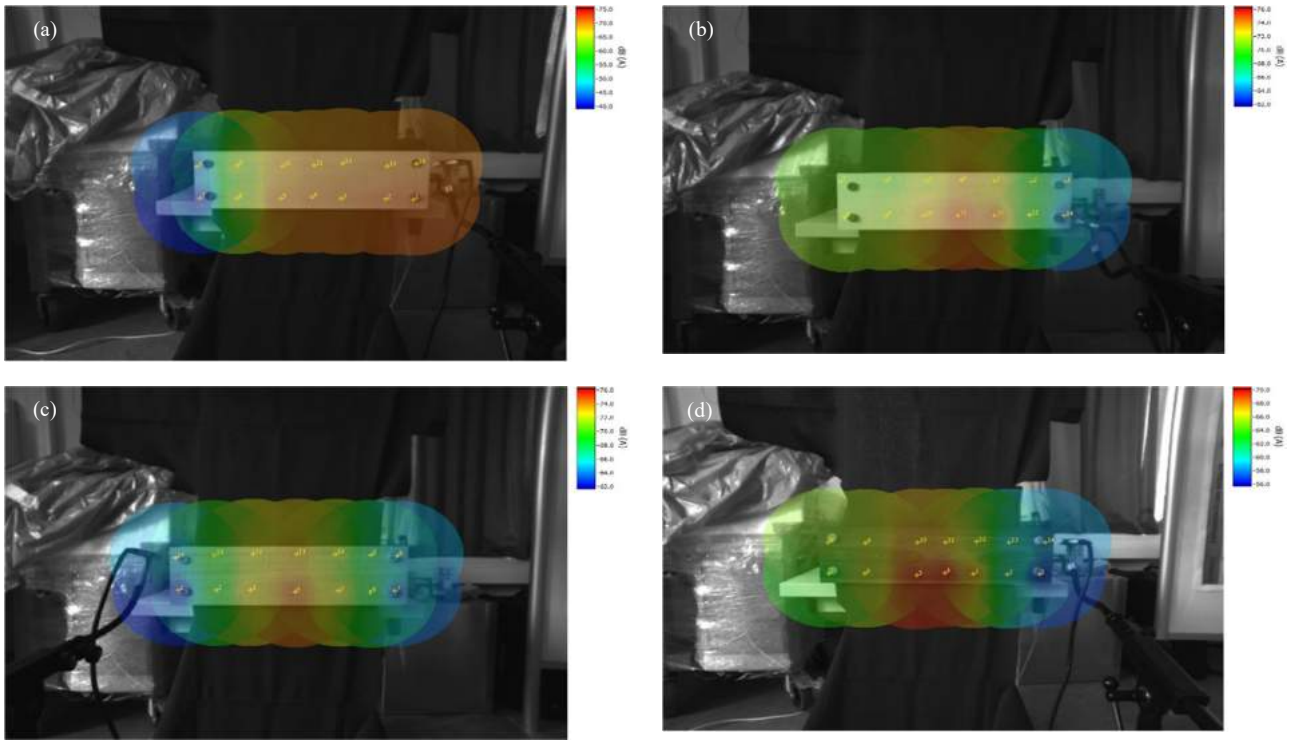

Fig. 7 Sound intensity distributions on wood sheets of European origin: (a) spruce, (b) maple latch, (c) oak latch, (d) cherry. Exciting frequency: 659.3 Hz.

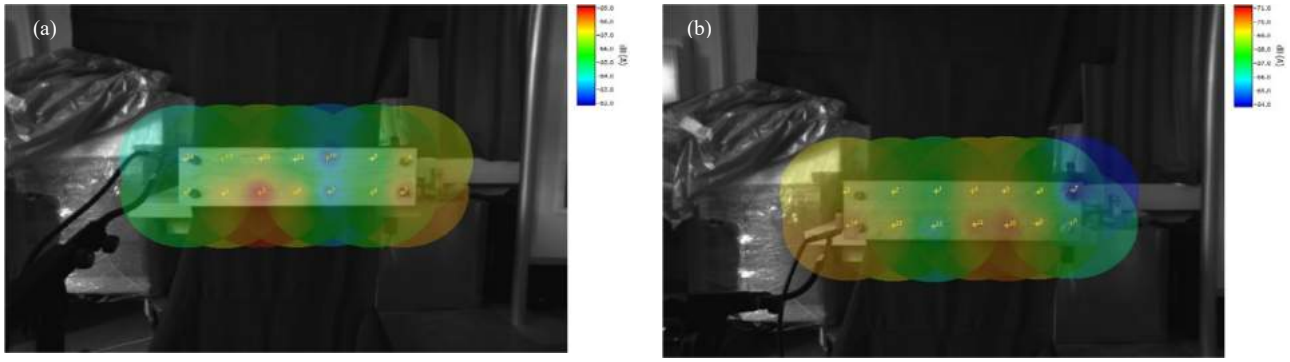

Fig. 8 Sound intensity distributions on wood sheets of American origin: (a) maple, (b) cherry. Exciting frequency: 659.3 Hz.

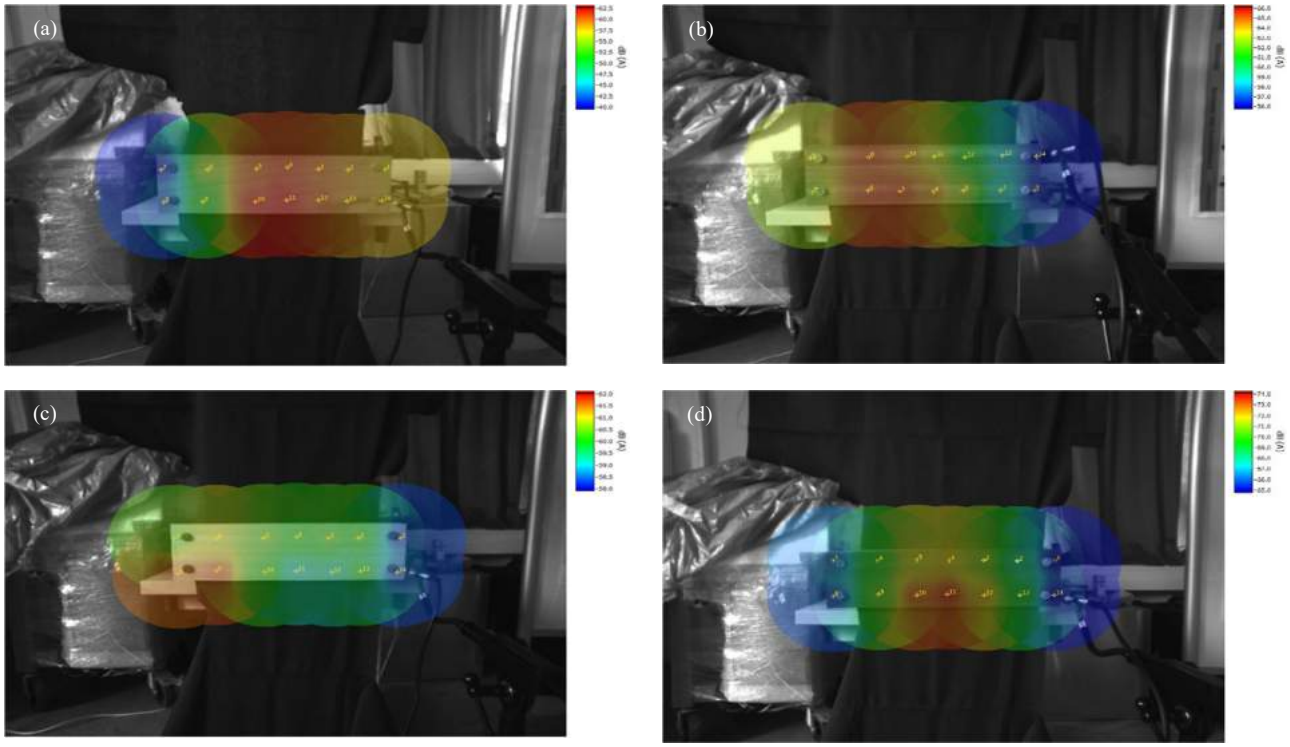

Fig. 9 Sound intensity distributions on wood sheets of African origin: (a) Khaya, (b) Padouk, (c) Abachi, (d) Wenge. Exciting frequency: 659.3 Hz.

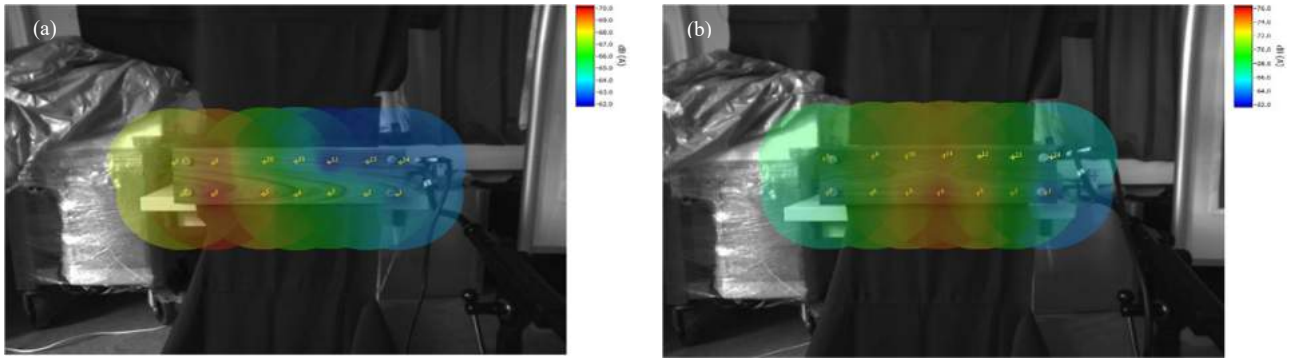

Fig. 10 Sound intensity distribution on wood sheets of South American origin: (a) Santos rosewood, (b) Ziricote. Exciting frequency: 659.3 Hz.

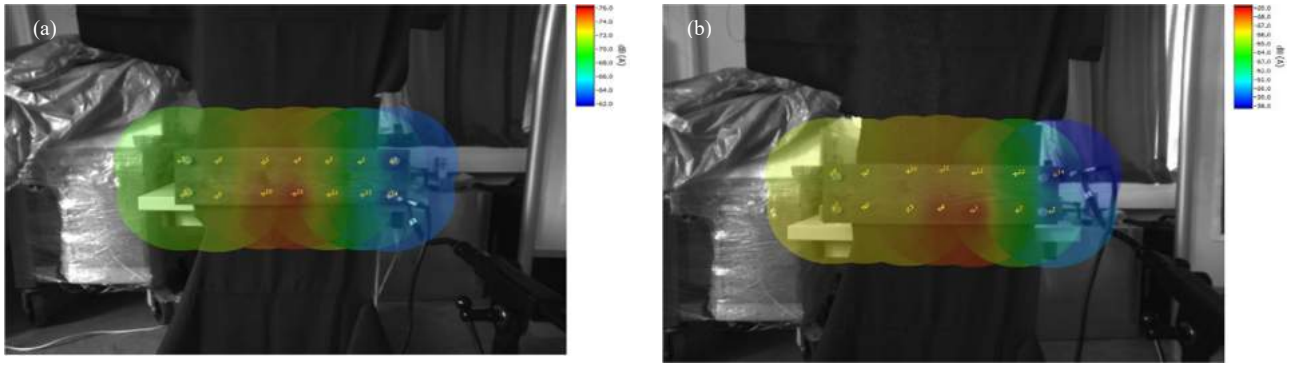

Fig. 11 Sound pressure distribution on wood sheets: (a) twisted, (b) untwisted Acacia. Exciting frequency: 659.3 Hz.

3 Data analysis

The resulting pictures from the used software (see Fig. 12 (a)), that produces colour-coded sound pressure values measured by the p-u sound probe on the surface of the wood sheets, were uploaded in a self-written image analysis program. Both, the analysis of a selected surface area or a line on the image were possible. A two-dimensional region of interest (ROI) on the image could be preselected (see Fig. 12 (b)), followed by the selection of a horizontal and/or a vertical line of interest (LOI) on the preselected area. A colour histogram was generated for the selection, including the total number of pixels for each RGB colour (red, green and blue) and the minimal, maximal and the mean RGB value. For the areal analysis, a three-dimensional relationship between the 2D position and the pixel value was investigated. The X- and Y-pixel positions start on the upper left corner at (0,0). A 3D curve smoothing was performed for a better visualisation of the sound distribution on the selected area of interest with the help of calculating the moving average of the RGB data. The animation of the 3D graph to be rotated or to change the positions of the axes enabled a specific determination of a further new selection of a smaller ROI. For the analysis along the selected line of interest, the horizontal or the vertical coordinate of the position had been kept constant and a two-dimensional relationship between the corresponding horizontal (X) or vertical (Y) position on the line and the pixel value of each of the RGB colours was plotted. Strongly inhomogeneous behaviour of the resulting curves could be a reference for an inhomogeneous sound distribution on the surface of a sample. The results should serve as a first rough estimation of the sound distribution's behaviour of some kinds of woods and thus their feasibility to be used as alternatives for common tonewoods.

(a) (b)

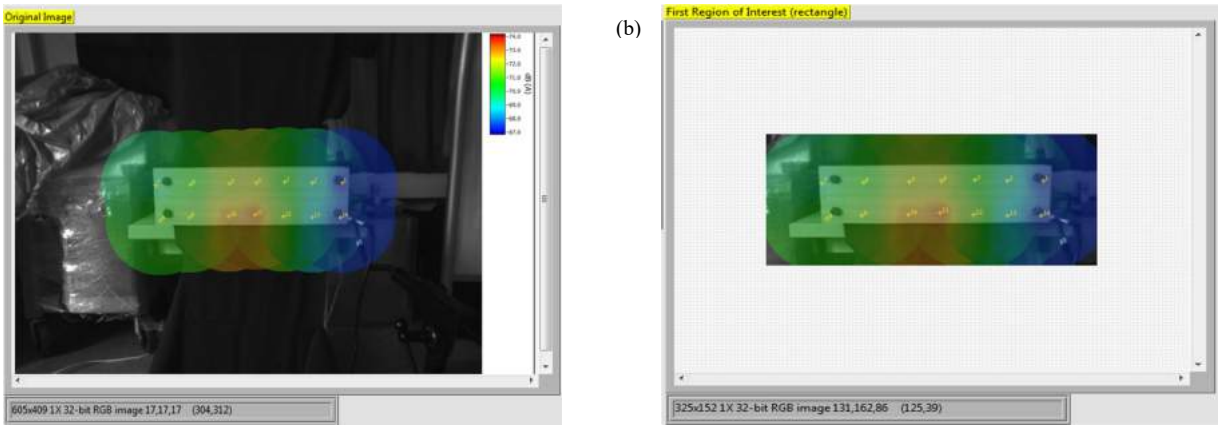

Fig. 12 Colour-coded sound pressure distribution on an Abachi wood sheet (exciting frequency: 220 Hz). (a) Original image, (b) rectangular ROI.

3.1 Data analysis of Abachi wood at an exciting frequency of 220 Hz

The following figures represent the resulting 3D graphs (before and after smoothing), the 2D graph representing the relationship between the X-position and the pixel value (RGB colours: r, g or b) at a constant Y-position, and the relationship between Y-position and the pixel value (r, g or b) at a constant X-position for the selected ROI (Fig.12 (b)) on the resulting colour-coded image of the sound pressure distribution on a sheet of Abachi wood due to an exciting frequency of 220 Hz.

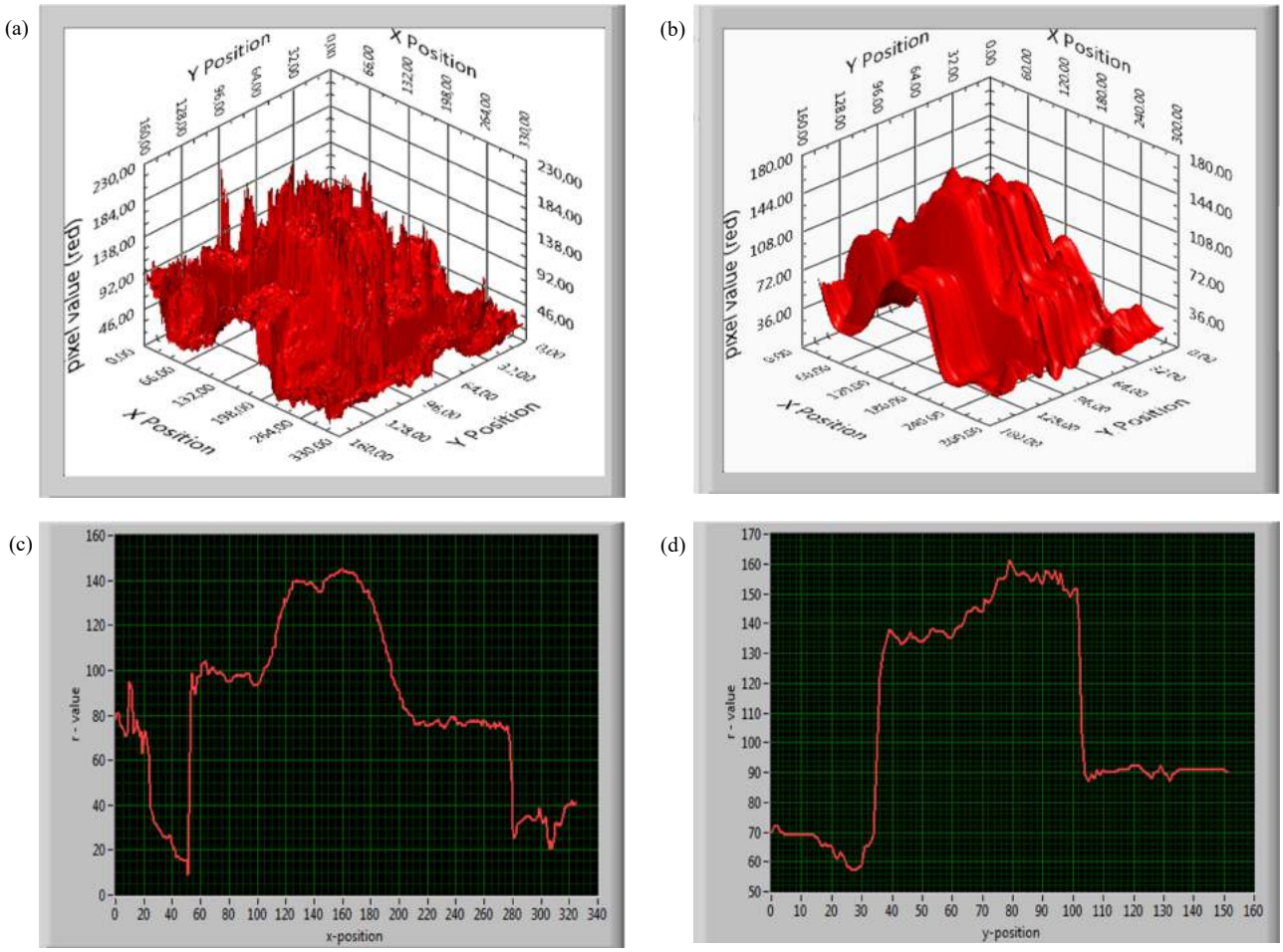

Fig. 13 Relationship between the X- and Y-position and pixel value on the ROI before (a) and after smoothing (b). Relationship between the position and the red-pixel value at a constant Y-position of 64 (c), as well as a constant X-position of 151 (d). Exciting frequency: 220 Hz.

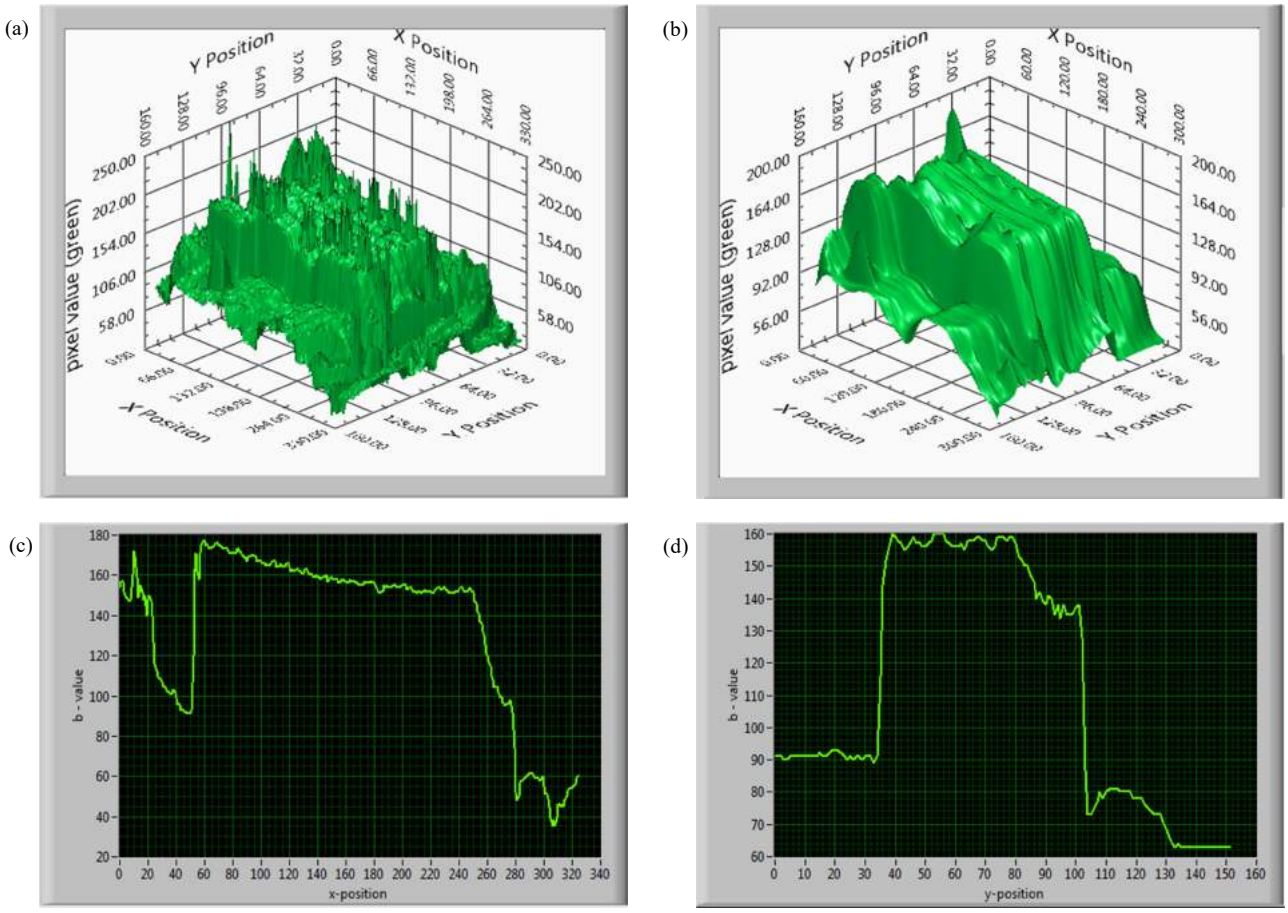

Fig. 14 Relationship between the X- and Y-position and pixel value on the ROI before (a) and after smoothing (b). Relationship between the position and the green-pixel value at a constant Y-position of 64 (c), as well as a constant X-position of 151 (d). Exciting frequency: 220 Hz.

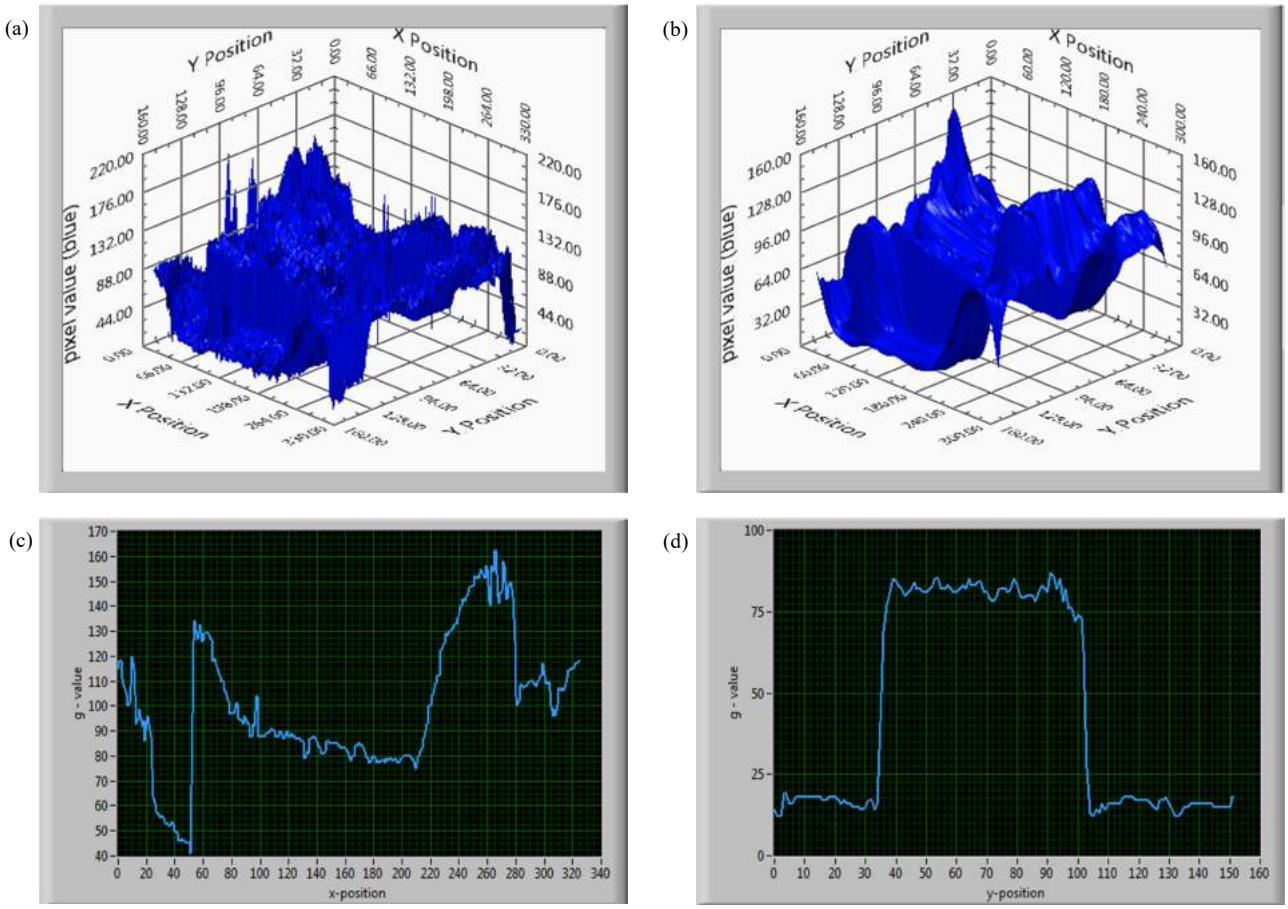

Fig. 15 Relationship between the X- and Y-position and pixel value on the ROI before (a) and after smoothing (b). Relationship between the position and the blue-pixel value at a constant Y-position of 64 (c), as well as a constant X-position of 151 (d). Exciting frequency: 220 Hz.

3.2 Comparison between the data analysis of African Khaya and American Cherry at an exciting frequency of 659.3 Hz

	African Khaya	American Cherry
original image and rectangular ROI	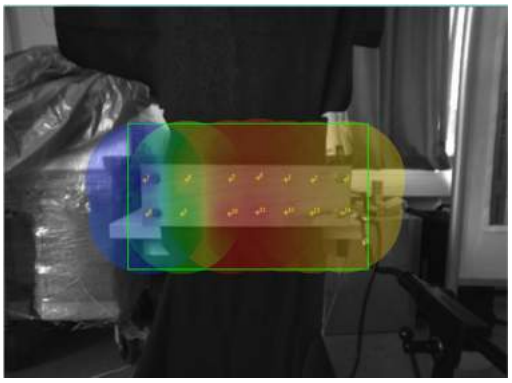	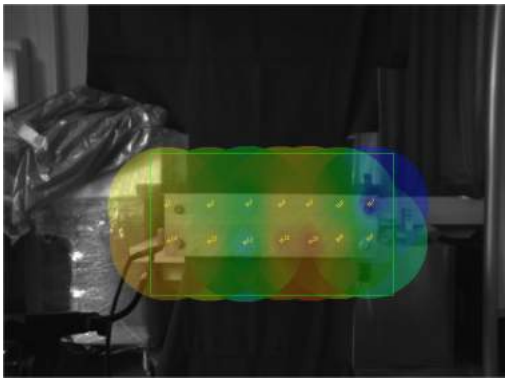
3D image analysis	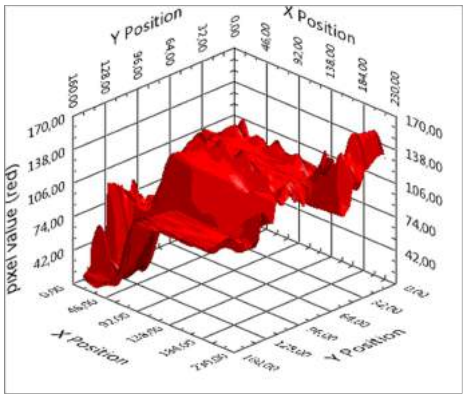	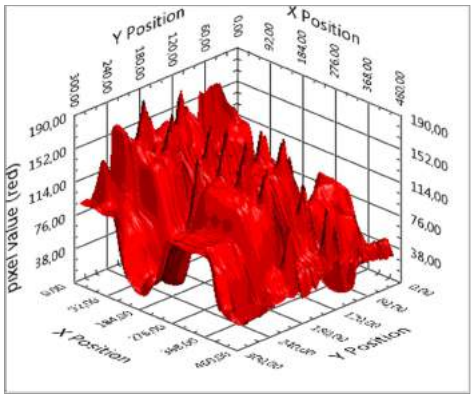
	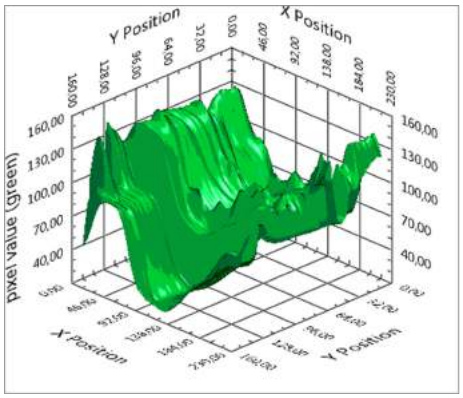	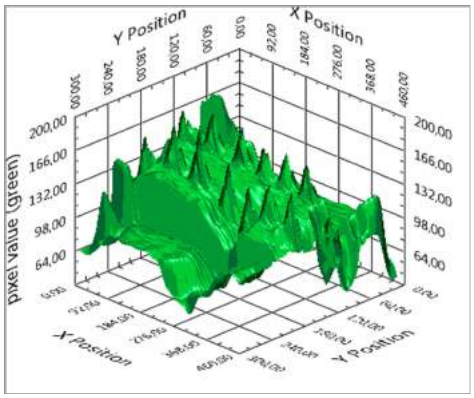
	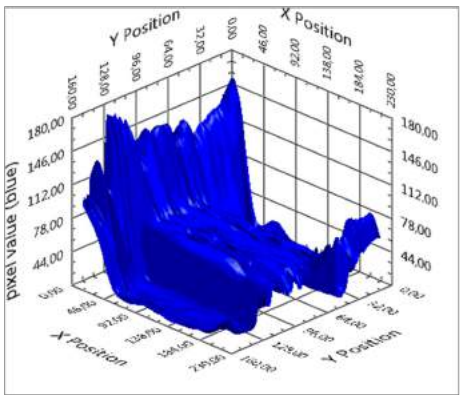	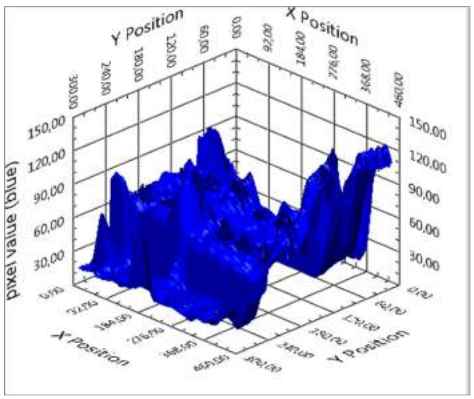

	African Khaya	American Cherry
horizontal LOI on the rectangular ROI	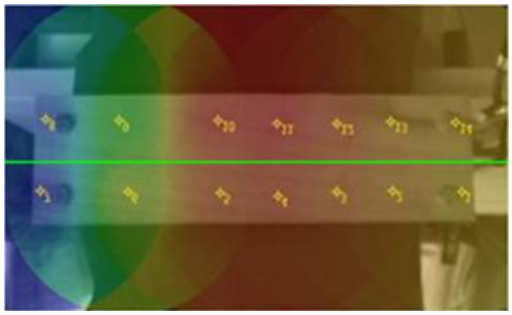	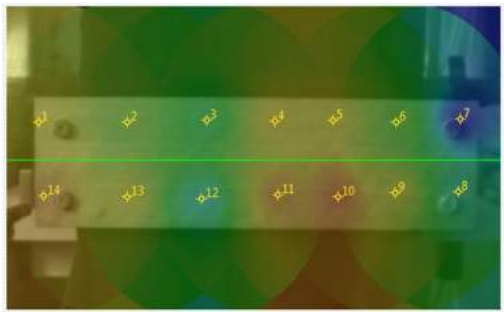
		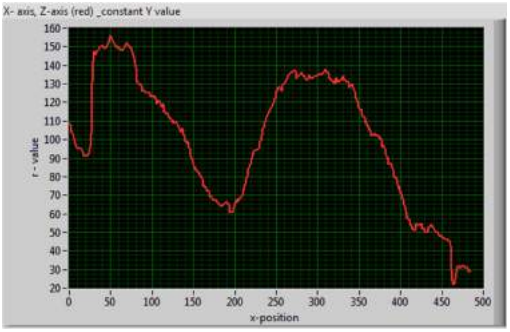
	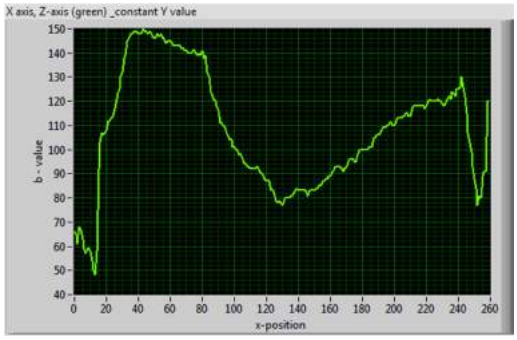	
	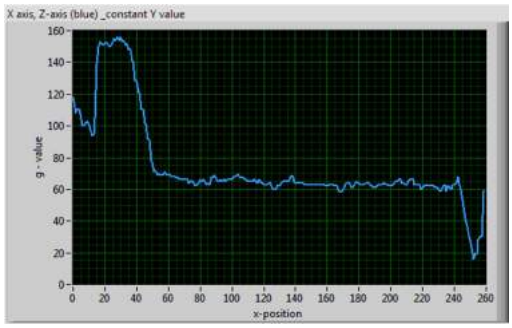	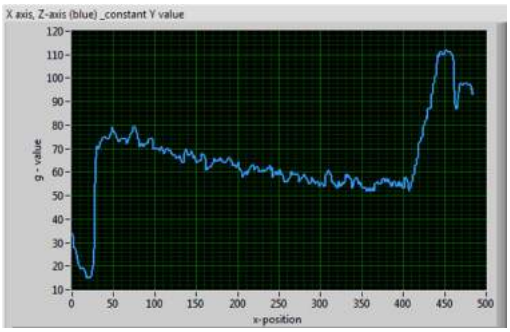

vertical LOI on the rectangular ROI

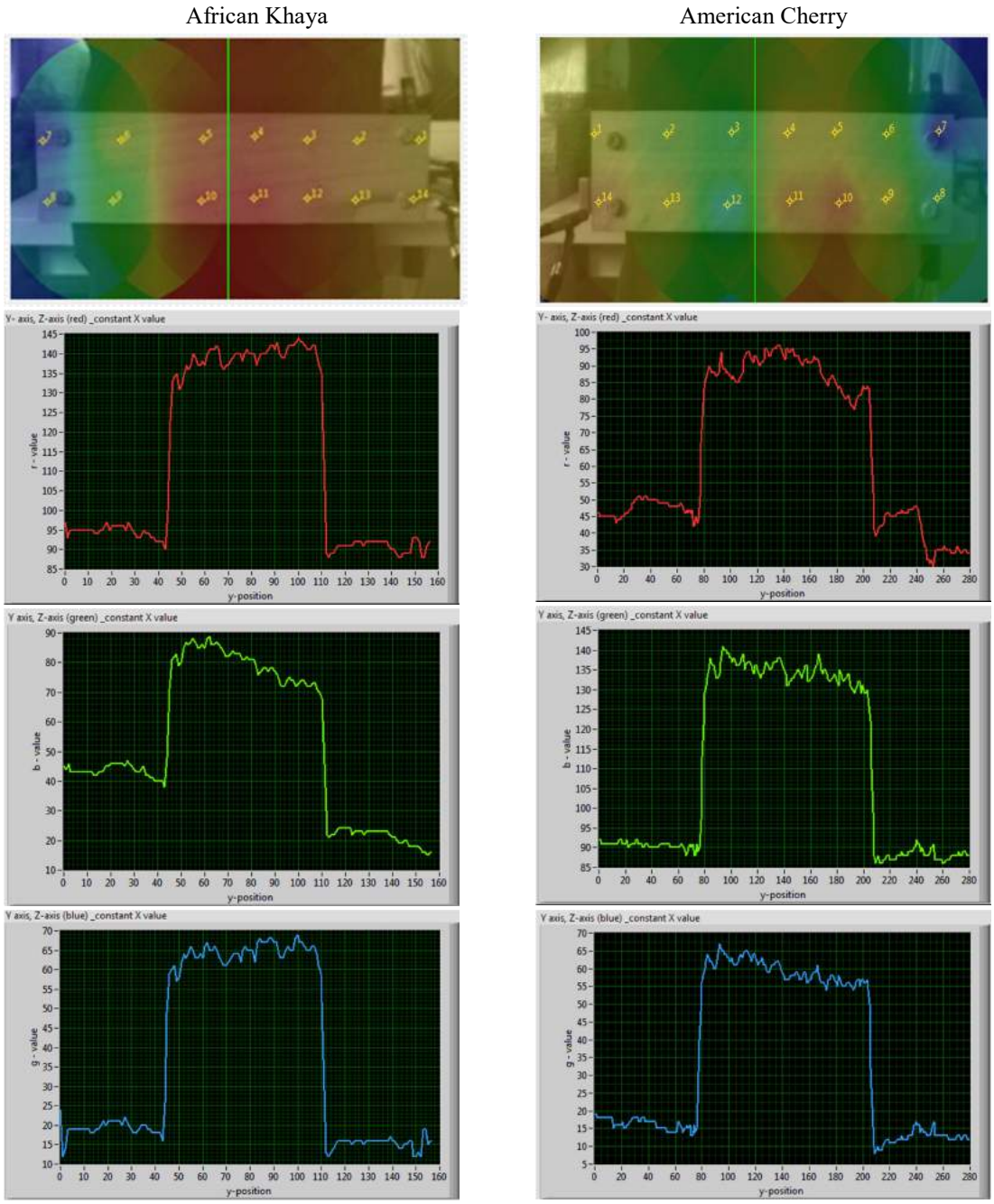

4 Summary and outlook

The investigation of colour-coded distribution of sound pressure on the surface of wooden samples using the mentioned equipment could be a reasonable way to gain a general impression about the difference in the sound qualities between different woods. This has been noticed by comparing the resulting images of the acoustic reactions of the wood sheets at constant exciting frequencies coming from the shaker using the presented image analysis for an objective evaluation of sound data. However, a further optimization of the experimental setup could provide more reliable results. This could be realized, for example, by an equal hanging of the wooden sheets on the frame at the 8 fixation points, with the help of light-weight force transducers. Furthermore, a correlation between the obtained results and the mechanical behaviour of the wooden sheets should improve the evaluation of the feasibility of using specific wood types in the intended applications.

5 Literature

[1] Madison, M.: Wood handbook - Wood as an Engineering Material. General Technical Report FPL-GTR-190, Forest Products Laboratory, United States Department of Agriculture Forest Service, USA (2010).

[2] Illegal Logging Portal, Major Impacts, Chatham House, London (2019). [Online]. Available: www.illegal-logging.info. [Accessed 20 February 2019].

[3] Hoare, A.: Tackling Illegal Logging and the Related TradeWhat Progress and Where Next? Chatham House, London (2015).

[4] Brown, C.: Working Paper No: GFPOS/WP/03, Forest Plantation Yields in the Tropical and Subtropical Zone. Food and Agriculture Organization of the United Nations, Rome, Italy (2000).

[5] Göken, J., Fayed, S., Schäfer, H., Enzenauer, J.: A Study on the Correlation between Wood Moisture and the Damping Behaviour of the Tonewood Spruce. Acta Physica Polonica A 133 (5), 1241-1260 (2018).

[6] Göken, J., Ahrends, H., Brink, H.: Use of a Sound Source Localisation System for the Experimental Determination of Vibration Patterns of a Square Plate. ARPN Journal of Engineering and Applied Sciences 9 (10), 1983-1993 (2014).

[7] van Honschoten, J.W.: Modelling and Optimisation of the Microflown. PhD thesis, University of Twente, the Netherlands (2004).

ISBN 978-3-944262-20-8